(NASA-CR-132437) A SOURCE FLOW CHARACTERISTIC TECHNIQUE FOR THE ANALYSIS OF SCRAMJET EXHAUST FLOW FIELD (Advanced Technology Labs., Inc., Westbury, N.Y.) 65 p HC $6.25

N74-22925

CSCL 20D G3/12

Unclas 39394

ADVANCED TECHNOLOGY LABORATORIES, INC.

NASA CR-132437

MARCH 1974

ATL TR 186

A SOURCE FLOW CHARACTERISTIC TECHNIQUE FOR THE ANALYSIS OF SCRAMJET EXHAUST FLOW FIELDS

By

P. Del Guidice, S. Dash
and P. Kalben

PREPARED FOR

NATIONAL AERONAUTICS AND SPACE ADMINISTRATION
LANGLEY RESEARCH CENTER
HAMPTON, VIRGINIA 23365

BY

ADVANCED TECHNOLOGY LABORATORIES, INC.
Merrick and Stewart Avenues
Westbury, New York 11590

I

INDEX

LIST OF FIGURES

LIST OF SYMBOLS

C_i = mole fraction

C_p = $C_p^*/C_{p\infty}$ specific heat

h = mixture enthalpy (equilibrium option - h^*/u_∞^2)

J_1 = 0 for two dimensional flow, 1 for axisymmetric flow

J_2 = 0 for two dimensional flow, 1 for axially expanding flow

L^* = reference length (throat height)

M = Mach number

m_i = molecular weight of i^{th} specie (frozen option)

n_i = molar concentration of i^{th} specie (frozen option)

NSP = number of species (frozen option)

p = $p^*/\rho_\infty u_\infty^2$ pressure

q = q^*/u_∞ velocity

R = mixture gas constant (fuel/air equivalence ratio for equilibrium option)

R_0 = universal gas constant

T = T^*/T_∞ temperature

W = average molecular weight of mixture (static enthalpy of mixture for equilibrium option, $W - h^*/u_\infty^2$)

x = x^*/L^* axial distance

y = y^*/L^* radial distance

α_i = mass fraction of i^{th} specie (frozen option)

γ = ratio of specific heats (equilibrium isentropic exponent for equilibrium option)

θ = flow inclination relative to the x axis

LIST OF SYMBOLS (Continued)

ρ = ρ^*/ρ_∞ density

μ = Mach angle

Th = Thrust (Th^{**}/L^{*2})

L = Lift (Lf^*/L^{*2})

My = Pitching Moment (My^*/L^{*3})

* = dimensional variables

∞ = free stream conditions (dimensional)

e = equilibrium

f = frozen

I. INTRODUCTION

The design and selection of a nozzle for a hypersonic scramjet must be based on a compromise between internal and external flow requirements related to vehicle lift, drag, pitching moment, thrust, structural and weight limitations. The design process involves a complex study based on engineering analysis and refinements using complex computer programs. A logical design sequence consists of first obtaining a satisfactory range of aerodynamic parameters utilizing simplified analysis[1,2,3] and then narrowing the range of parameters through more accurate but complex calculations.

This report describes a two dimensional second-order characteristic procedure capable of analyzing the aerodynamic performance of typical nozzle configurations selected from simplified analysis as shown in Figure (1).

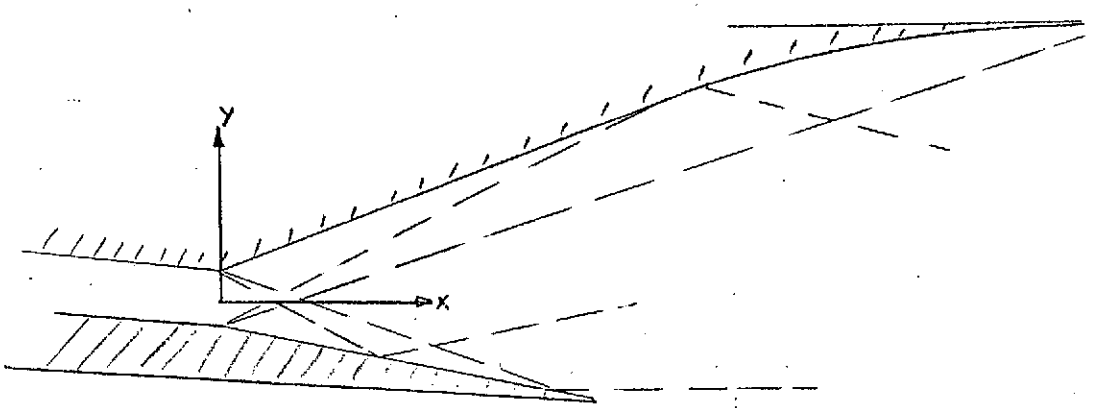

FIGURE 1. TYPICAL SCRAMJET NOZZLE

However, the calculation procedure is not limited to these configurations but can be readily adapted to calculate other two dimensional configurations. This generality results from the use of three coordinates systems, axisymmetric, axially expanding (source type flow) and Cartesian (plane two dimensional). Automatic provisions for switching from axially expanding to Cartesian coordinates at a specified axial station and multiple source origins are provided for as a user option. This unique feature allows the lateral nozzle area variation, as in Figure (2), to be accounted for in a quasi-two dimensional manner.

A higher order calculation would involve a fully three dimensional calculation which would locate the lateral waves.

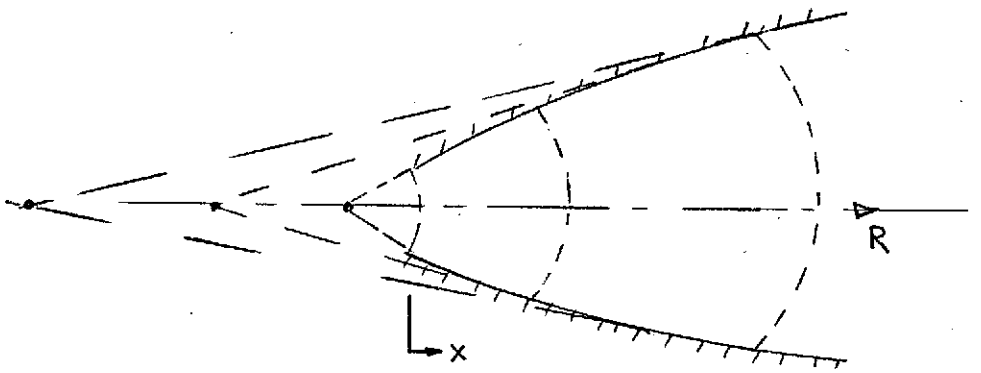

FIGURE 2. MULTIPLE SOURCE ORIGINS FOR LATERAL NOZZLE AREA VARIATION.

The working fluid is assumed to be a hydrogen-air mixture in frozen or chemical equilibrium. The mixture thermodynamics is expressed via curve fits; i.e., individual species curve fits for frozen flow[4] and mixture fits for equilibrium flow[5].

The following boundary conditions are provided for in the calculation.

(1) Wall boundaries
(2) Shock boundaries (Equilibrium flow only)
(3) Contact surface (Equilibrium with shock only)
(4) Underexpansion interaction (Equilibrium only)
(5) Overexpansion interaction (Equilibrium only)
(6) Prandtl-Meyer (Equilibrium only)

While the nozzle may be over or underexpanded at the cowl, as a user option no external interaction need be selected. It is always assumed that the nozzle has a centerbody or lower wall,

As part of the calculation a running integration of pressure on the nozzle surfaces is performed which yields thrust, lift and pitching moment in vehicle coordinates. The pitching moment calculation requires the location of the moment axis to be specified. Appendix III illustrates the method.

Section II (a,b) describes the basic flow equations for a rotational non-homoentropic gas-mixture. The derivation of the characteristic equations is given in Appendix I and the thermodynamic curve fit data is given in Appendix II. Section II(c) describes the numerical scheme and grid employed, while Section III discusses the various boundary conditions. Some sample calculations are presented in Section IV, and Section VI contains concluding remarks. Reference (7) contains a description of the program and a sample input.

II. BASIC EQUATIONS

A. Frozen Chemistry - The equations governing the two dimensional, axisymmetric, or axially expanding inviscid flow of a gas mixture, with frozen chemistry, may be written as follows:

Continuity:
$$\frac{\partial(\rho q)}{\partial s} + \rho q \frac{\partial \theta}{\partial n} + J_1 \frac{\rho q}{y} \sin\theta + J_2 \frac{\rho q}{x} \cos\theta = 0 \tag{1}$$

S-Momentum:
$$\rho q \frac{\partial q}{\partial s} + \frac{\partial p}{\partial s} = 0 \tag{2}$$

N-Momentum:
$$\rho q^2 \frac{\partial \theta}{\partial s} + \frac{\partial p}{\partial n} = 0 \tag{3}$$

Energy:
$$\frac{1}{(\gamma_\infty - 1) M_\infty^2} C_p \rho q \frac{\partial T}{\partial s} - q \frac{\partial p}{\partial s} = 0 \tag{4a}$$

Species Conservation:
$$\frac{\partial \alpha_i}{\partial s} = 0 \quad (i=1, NSP) \tag{5a}$$

State:
$$p = \frac{\rho T}{W} \frac{W_\infty}{\gamma_\infty M_\infty^2} \tag{6a}$$

where J_1 and J_2 are the axisymmetric and axially expanding (source) terms respectively. By straightforward algebraic maniupulation, the above equations may be cast into characteristic form (as done in Appendix I).

Let C_+ denote an up-running and C_- denote a down-running characteristic. Then, along a $C_\pm$ characteristic, whose slope is expressed by:

$$\frac{dy}{dx} = \tan(\theta \pm \mu_f) \tag{7a}$$

the compatibility relation may be written

$$\frac{\sin\mu_f \cos\mu_f}{\gamma_f} d \ln p \pm d\theta + \left(J_1 \frac{\sin\theta}{y} + J_2 \frac{\cos\theta}{x}\right) \frac{\sin\mu_f}{\cos(\theta \pm \mu_f)} dx = 0^* \tag{8a}$$

* The use of d(LnP) in place of $\frac{dP}{p}$ considerably improves the accuracy of the results for a given mesh spacing.

It is to be noted that at a point in the flow (x,y), the properties are completely specified by q, T, p, θ and α_i (i=1, NSP). Other variables may be calculated as follows.

The molecular weight is expressed by

$$W = \left(\Sigma \frac{\alpha_i}{m_i} \right)^{-1} \tag{9}$$

hence the mixture's gas constant is

$$R = \frac{R_0}{W}$$

The density is obtained from the equation of state

$$\rho = \frac{WP}{T} \frac{\gamma_\infty M_\infty^2}{W_\infty}$$

The thermodynamic properties $C_{p_i}(T)$, $h_i(T)$ and $s_i(T)$ are tabulated polynomials, a description of which may be found in Appendix II.

The specific heat of the mixture is expressed by

$$C_{p_f} = \sum_{i=1}^{NSP} C_{p_{i_f}} \alpha_i \tag{10}$$

and the ratio of specific heats by

$$\gamma_f = \frac{C_{p_f}}{C_{p_f} - R/C_{p_\infty}} \tag{11}$$

The local frozen Mach number is

$$M_f = \frac{M_\infty q}{\sqrt{T}} \left(\frac{\gamma_\infty R_\infty}{\gamma R} \right)^{\frac{1}{2}} \tag{12}$$

and the Mach angle is given by

$$\mu_f = \sin^{-1} \frac{1}{M_f} \tag{13a}$$

B. Equilibrium Chemistry - The equations governing the two dimensional, axisymmetric, or axially expanding inviscid flow of a gas mixture in chemical equilibrium may be written as follows:

Continuity: $$\frac{\partial}{\partial s}(\rho q) + \rho q \frac{\partial \theta}{\partial n} + J_1 \rho q \frac{\sin\theta}{y} + J_2 \rho q \frac{\cos\theta}{x} = 0 \quad (1)$$

S-Momentum: $$\rho q \frac{\partial q}{\partial s} + \frac{\partial p}{\partial s} = 0 \quad (2)$$

N-Momentum: $$\rho q^2 \frac{\partial \theta}{\partial s} + \frac{\partial p}{\partial n} = 0 \quad (3)$$

Conservation of Stagnation Enthalpy: $$\frac{\partial H}{\partial s} = 0 \quad \text{where } H = h + \frac{1}{2} q^2 \quad (4b)$$

Constancy of Equivalence Ratio Along Streamlines: $$\frac{\partial \Phi}{\partial s} = 0 \quad (5b)$$

Caloric Equation of State: $$p/\rho^{\Gamma} = \text{constant} \quad (6b)$$

where the equilibrium isentropic exponent is given by

$$\Gamma = f(h, p, \Phi)^* \quad (14)$$

Then along the $C_{\pm}$ characteristic whose slope is given by

$$\frac{dy}{dx} = \tan(\theta \pm \mu_e) \quad (7b)$$

the compatibility relation may be written as

$$\frac{\sin\mu_e \cos\mu_e}{\Gamma} d \ln p \pm d\theta + \left(J_1 \frac{\sin\theta}{y} + J_2 \frac{\cos\theta}{x}\right) \frac{\sin\mu_e}{\cos(\theta \pm \mu_e)} dx = 0 \quad (8b)$$

Thus, at a point (x,y) in the flow the properties q, h, p, ρ, Γ, Φ,θ are known.

*Fits for Γ have been expressed in polynomial form from properties tabulated in Reference (5) as described in Appendix II.

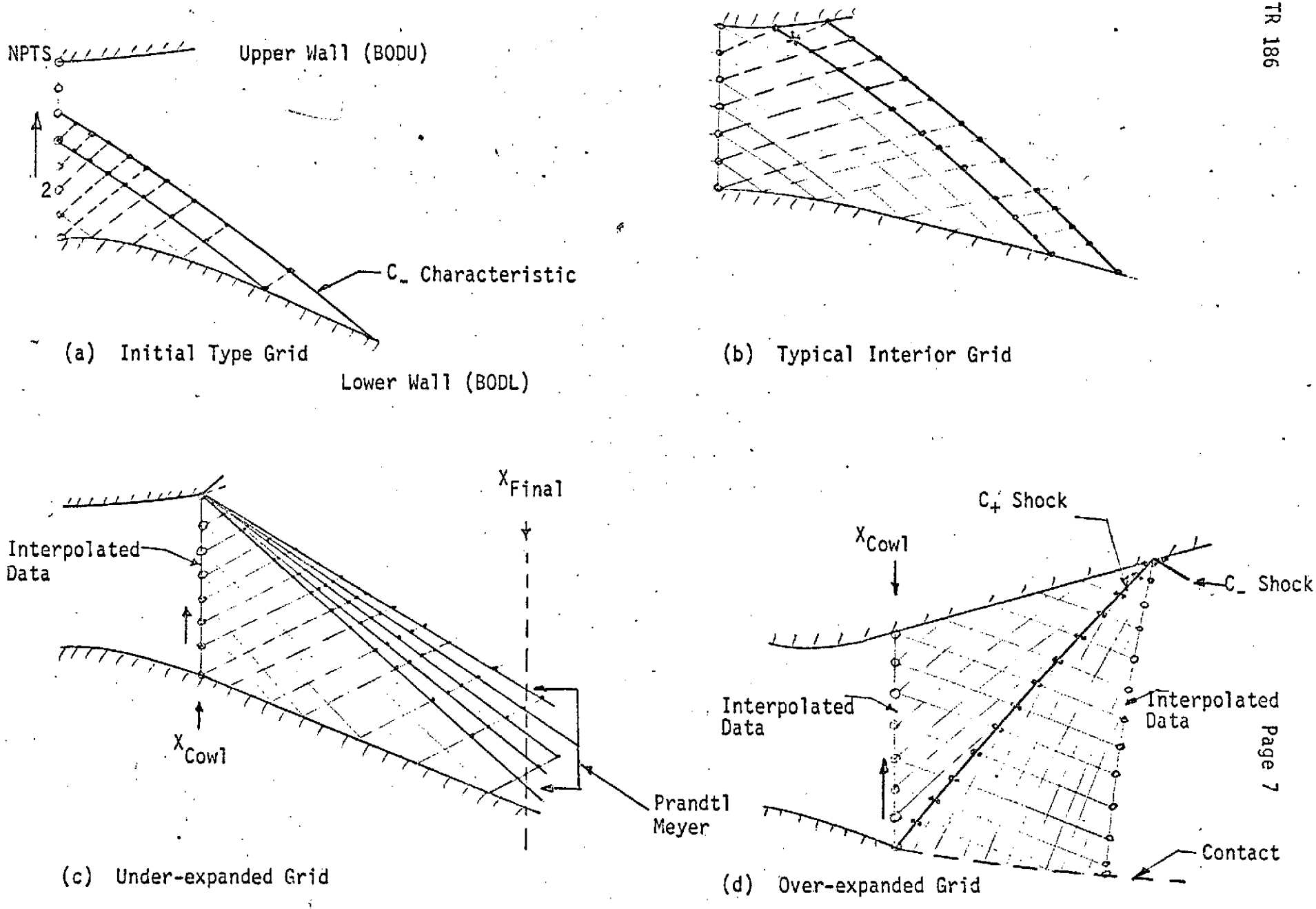

FIGURE 3. TYPICAL GRIDS

The local equilibrium Mach number and Mach angle are given by

$$M_e = q/a_e \tag{15}$$

and

$$\mu_e = \sin^{-1} \frac{1}{M_e} \tag{13b}$$

where

$$a_e^2 = \Gamma\, p/\rho \tag{16}$$

C. Numerical Procedure and Characteristic Network - Figure (3) depicts the global grid ordering scheme used in the present program. While a free running characteristic network is used the program orders and stores data along down-running (C_-) characteristics[6]. The only exception being the initial data line which must be a non-characteristic line. The marching proceeds from one C_- line to another until the desired flow field is calculated.

A typical characteristic mesh is depicted in Figure (4), properties being known along the line AB and to be determined at the point C.

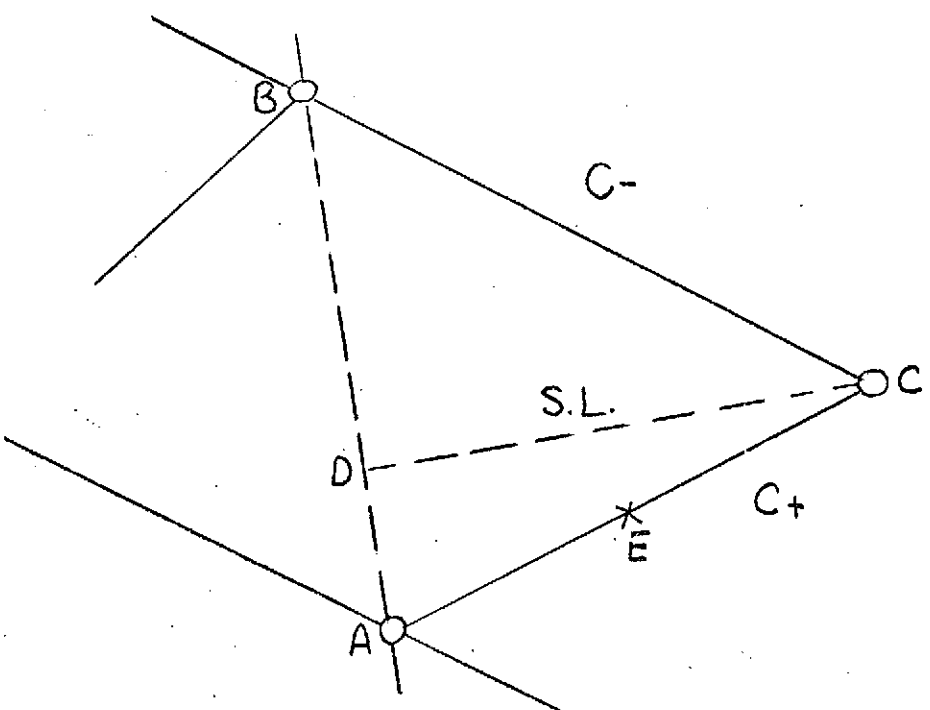

FIGURE 4. CHARACTERISTIC MESH

Let

$$M_1 = \alpha \tan(\theta+\mu)_A + \beta \tan(\theta+\mu)_C \tag{17a}$$

$$M_2 = \alpha \tan(\theta-\mu)_B + \beta \tan(\theta-\mu)_C \tag{17b}$$

and

$$M_3 = \alpha \tan \theta_D + \beta \tan \theta_C \tag{17c}$$

The Mach angles (μ) are the local values corresponding to either frozen or equilibrium flow. The α and β in the above and following equations are used as artifices in averaging properties along characteristics. In a first approximation α would be set equal to one and β equal to zero, thus fixing values at the points A, B or D. Once properties at point C are determined, the coefficients involved in the calculation are averaged by setting both α and β equal to one-half. This corresponds to the second iteration. Writing Equation (7) in finite difference form

$$\frac{y_C-y_A}{x_C-x_A} = M_1 \tag{18a}$$

and

$$\frac{y_C-y_B}{x_C-x_B} = M_2 \tag{18b}$$

Solving the above yields

$$x_C = \frac{y_B-y_A+M_1x_A-M_2x_B}{M_1-M_2} \tag{19a}$$

$$y_C = y_A + M_1(x_C-x_A) \tag{19b}$$

For frozen flow let

$$A_1 = \alpha\left(\frac{\sin\mu \cos\mu}{\gamma}\right)_A + \beta\left(\frac{\sin\mu \cos\mu}{\gamma}\right)_C \tag{20a}$$

$$B_1 = \left(\frac{\sin\mu \cos\mu}{\gamma}\right)_B + \beta\left(\frac{\sin\mu \cos\mu}{\gamma}\right)_C \tag{20b}$$

for equilibrium flow the Mach number and angles μ are the local equilibrium values and the ratio of specific heats γ is replaced by the equilibrium exponent Γ. Similar remarks apply to all further characteristic coefficients.

$$A_2 = J_1 \left[\alpha\left(\frac{\sin\theta \sin\mu}{y \cos(\theta+\mu)}\right)_A + \beta\left(\frac{\sin\theta \sin\mu}{y \cos(\theta+\mu)}\right)_C\right] \tag{21a}$$

$$+ J_2 \left[\alpha\left(\frac{\cos\theta \sin\mu}{x \cos(\theta+\mu)}\right)_A + \beta\left(\frac{\cos\theta \sin\mu}{x \cos(\theta+\mu)}\right)_C\right] \tag{21b}$$

$$B_2 = J_1 \left[\alpha\left(\frac{\sin\theta \sin\mu}{y \cos(\theta-\mu)}\right)_B + \beta\left(\frac{\sin\theta \sin\mu}{y \cos(\theta-\mu)}\right)_C\right] \tag{21c}$$

$$+ J_2 \left[\alpha\left(\frac{\cos\theta \sin\mu}{x \cos(\theta-\mu)}\right)_B + \beta\left(\frac{\cos\theta \sin\mu}{x \cos(\theta-\mu)}\right)_C\right] \tag{21d}$$

Hence, along AC (C_+ characteristic)

$$A_1 (\ln p_C - \ln p_A) + \theta_C - \theta_A + A_2 (x_C - x_A) = 0 \tag{22a}$$

and along BC (C_- characteristic)

$$B_1 (\ln p_C - \ln p_B) - \theta_C + \theta_B + B_2 (x_C - x_B) = 0 \tag{22b}$$

Solving the above equations for $\ln p_C$ yields

$$\ln p_C = (A_1 \ln p_A + B_1 \ln p_B + \theta_A - \theta_B - (A_2+B_2) x_C + A_2 x_A + B_2 x_B)/(A_1 + B_1) \tag{23}$$

hence $p_C = \exp(\ln p_C)$ and the flow inclination is

$$\theta_C = \theta_A - A_1 (\ln p_C - \ln p_A) - A_2 (x_C - x_A) \tag{24}$$

If either the entropy or stagnation enthalpy is not constant throughout the flow field, the streamlines are the third family of characteristics, whose

slope is given by

$$\frac{dy}{dx} = \tan \theta \tag{25}$$

Then, in difference form,

$$\frac{y_C - y_D}{x_C - x_D} = M_3 \tag{26}$$

Referring to Figure (4), the point D lies between points A and B and can be located by an iterative procedure using Equation (26). Properties at point D are then obtained by linearly interpolating between A and B.

The velocity at point C is found using the S-Momentum equation in the form;

$$q_C = q_D - \frac{2(p_C - p_D)}{[\alpha(\rho q)_D + \beta(\rho q)_C]} \tag{27}$$

If the chemistry is frozen the temperature may be obtained using the Energy Equation (4a) along CD. That is

$$T_C = T_D + \frac{(\gamma_\infty - 1)M_\infty^2 (p_C - p_D)}{\alpha(\rho C_p)_D + \beta(\rho C_p)_C} \tag{28}$$

The Species Conservation Equation (4a) yields

$$\alpha_{i_C} = \alpha_{i_D} \quad (i = 1, NSP) \tag{29}$$

and the remaining variables are found using Equations (6a) through (13a).

If the chemistry is in equilibrium the Energy Equation (4b) yields the static enthalpy

$$h_C = h_D + (q_D^2 - q_C^2)/2 \tag{30}$$

and the constancy of equivalence ratio along streamlines yields

$$\Phi_C = \Phi_D \tag{31}$$

the curve fits for the isentropic exponent Γ yield

$$\Gamma_C = \Gamma(p_C, h_C, \Phi_C) \tag{14}$$

and the State Equation (6b) yields the density.

The remaining variables are obtained from Equations (13b), (15) and (16). The calculation is then repeated with the coefficients averaged, by setting α and β equal to 1/2. If properties change significantly between these two sets of calculations, this generally implies too large a mesh in this region.

III. BOUNDARY CALCULATIONS

A. Upper Or Lower Wall - The nozzle wall shapes, either upper wall (cowl) or lower wall (vehicle undersurface) are specified by polynomials of the form

$$y_j = A_j(x-x_i)^2 + B_j(x-x_i) + C_j \tag{32a}$$

where x_i is the origin of the wall. A maximum of 3 wall segments are permitted, i.e., $j = 3$. The wall slope θ_w is given by

$$\tan \theta_w = 2A_j(x-x_i) + B_j \tag{32b}$$

In Figure (5), DC is the specified upper nozzle wall. The point A lies on

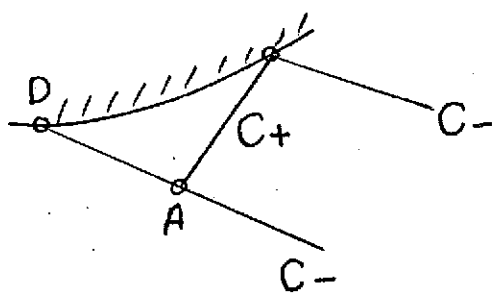

FIGURE 5. WALL POINT

the C_- characteristic DA on which all properties are known and point C is located for $\alpha = 1$ and $\beta = 0$ by a simultaneous solution of Equation (32a) and

$$\frac{y_C-y_A}{x_C-x_A} = \alpha \tan(\theta+\mu)_A + \beta \tan(\theta+\mu)_C = M_1 \tag{33}$$

Note that this solution involves a minor iteration since (x_C, y_C) and hence $\theta_C = \theta_w(x_C)$ are not known a priori.

Having located point C, θ_C is known and the compatibility relation along AC, i.e., Equation (22a) determines the pressure p_C

$$\ln p_C = \ln p_A + \frac{\theta_A - \theta_C - A_2(x_C - x_A)}{A_1}; p_C = \exp(\ln p_C) \tag{34}$$

the streamline equations applied along DC for either frozen or equilibrium flow then determine the remaining flow variables. The process is then repeated for $\alpha = \frac{1}{2}$, $\beta = \frac{1}{2}$. Similar remarks apply for a lower wall calculation except the characteristic relation (Equation 22b) is applied along a down characteristic (C_-).

B. Shock Phenomena - The program developed has the capability of computing the shock strength associated with an inviscid supersonic over or under-expansion process, and a shock propagating into a nonuniform media.

1. Hugoniot Relations - Assume a coordinate system oriented along ($\hat{t}$ direction) and normal to the shock surface ($\hat{n}$ direction) as shown in Figure (6). The angle sigma σ is the direction cosine of the shock with respect to the Cartesian direction x, and $\tilde{u}$ and $\tilde{v}$ are the velocity components in the $\hat{n}$ and $\hat{t}$ directions.

$$\hat{n} = -\sin\sigma i_x + \cos\sigma i_y \tag{35}$$

$$\hat{t} = \cos\sigma i_x + \sin\sigma i_y \tag{36}$$

$$\vec{V} = -\tilde{u}\,\hat{n} + \tilde{v}_t\,\hat{t} = u\hat{i}_x + v i_y \tag{37}$$

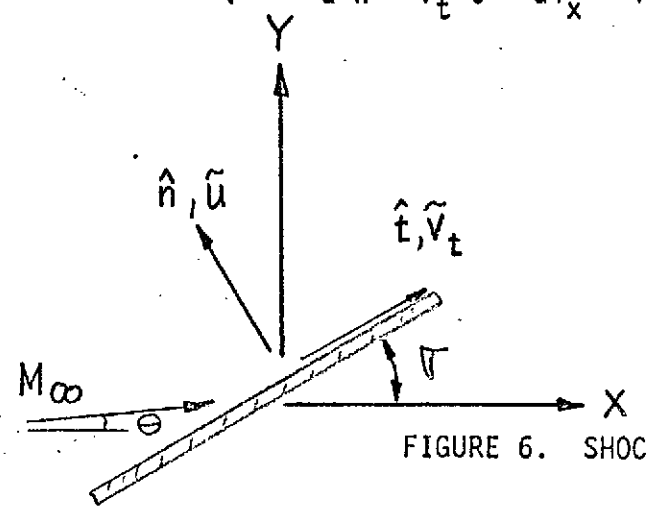

$$\hat{n} = -\sin\sigma i_x + \cos\sigma i_y$$
$$\hat{t} = \cos\sigma i_x + \sin\sigma i_y$$
$$\vec{M}_\infty = -M_n\,\hat{n} + M_t\,\hat{t}$$
$$\vec{M}_\infty = M_\infty(\cos\theta i_x + \sin\theta i_y)$$

FIGURE 6. SHOCK COORDINATES

The Rankine Hugoniot relations for a mixture in chemical equilibrium take the form

Continuity: $$\rho_1 \tilde{u}_1 = \rho_2 \tilde{u}_2 \quad (38)$$

Normal Momentum: $$p_1 + \rho_1 \tilde{u}_1^2 = p_2 + \rho_2 \tilde{u}_2^2 \quad (39)$$

Tangential Momentum: $$\tilde{v}_{t_1} = \tilde{v}_{t_2} \quad (40)$$

Energy: $$H = h + \frac{1}{2} V^2 = \text{constant} \quad (41)$$

State: $$\rho = \rho(p, h, \Phi_1) \quad (42)$$

where $$\Phi = \text{constant} \quad (43)$$

Employing the jump relations for a given shock angle and upstream conditions requires an iteration process since the mixture is calorically imperfect.

Let 1 designate upstream conditions and 2 downstream conditions. To solve the jump relations knowing conditions at 1, a value for $\tilde{u}_2$ is assumed. The density ρ_2 is computed using Equation (38), p_2 is computed using Equation (39) and Equation (41) yields a value for h_2. The State Equation (42) then yields an alternate value for the density. If this value for density does not agree with that calculated from continuity to within a specified tolerance, a new value of $\tilde{u}_2$ is assumed and this process is repeated until convergence is achieved.

2. Shock Point Calculation - Referring to Figure (7), a typical shock wave calculation is performed as follows. A value of the shock angle σ_c is assumed, and a simultaneous solution of the equations

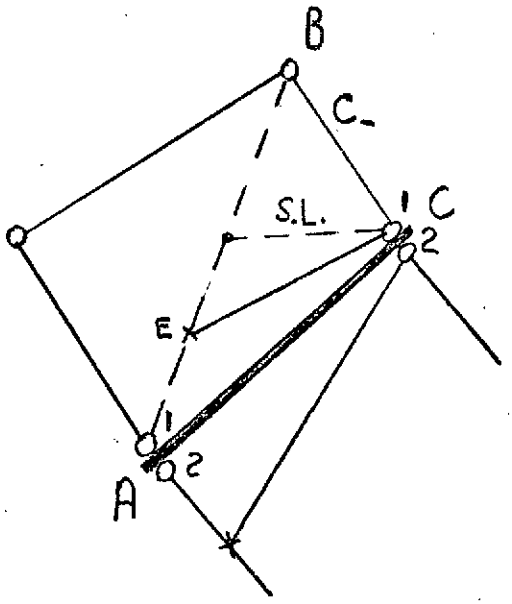

FIGURE 7. SHOCK POINT CALCULATION

$$\frac{y_C - y_{A_1}}{x_C - x_{A_1}} = \frac{1}{2}(\tan \theta_C + \tan \theta_{A_1})$$

and

$$\frac{y_C - y_B}{x_C - x_B} = M_2$$

yields x_C, y_C.

Since this flow is nonuniform a characteristic calculation similar to an interior point calculation yields the flow properties at C_1. Note that point E on the C_+ characteristic EC_1 is interpolated between B and A_1. The jump relations (Equations 38 - 43) are solved using the determined upstream conditions based on the assumed angle σ_C. This yields all properties at C_2. Using the deflection angle θ_{C_2} calculated from the jump conditions, a C_+ characteristic calculation performed along $(F\text{-}C_2)$ yields an alternate value of the pressure at p_{C_2}. The pressures are compared and if the difference exceeds a specified tolerance, a new value of σ_C is assumed and the process repeated until convergence is obtained. After convergence with

$\alpha = 1$, $\beta = 0$, the calculation is repeated using $\alpha = \frac{1}{2}$, $\beta = \frac{1}{2}$.

C. Under-Expansion Interaction - The program developed has the capability for equilibrium flows of computing the under-expansion interaction produced by pressure mismatch between the nozzle and a surrounding airstream. This situation is depicted in Figure (8a). Under-expansion conditions occur

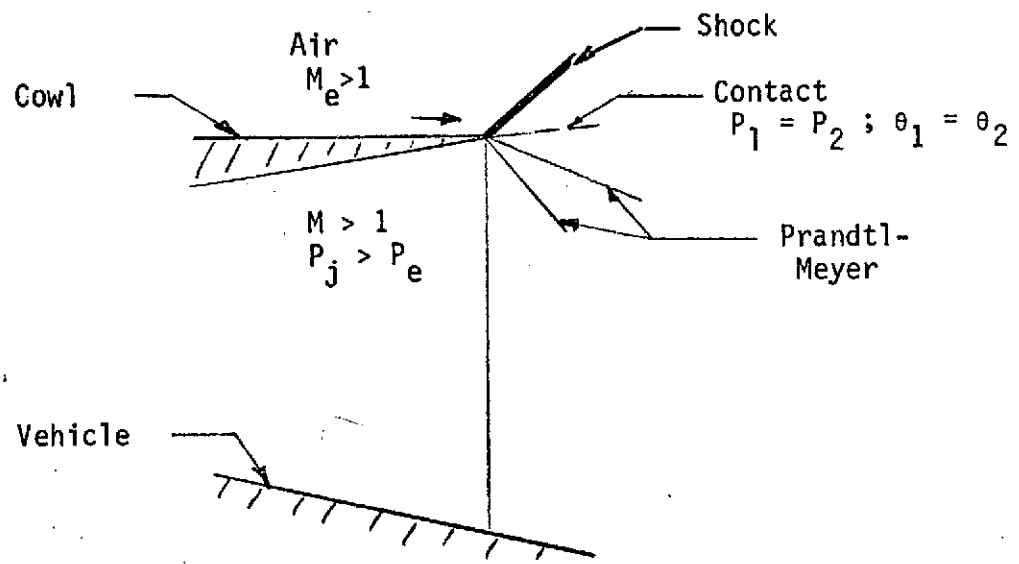

FIGURE 8a. UNDER-EXPANSION INTERACTION

as a result of either $P_j > P_e$ or $\theta_j > \theta_e$ or some combination of both conditions. Generally $P_j >> P_e$ defines an under-expanded flow. It is assumed that during the under-expansion interaction, the species remain chemically in equilibrium. The expansion is isentropic and the local interaction is two dimensional and inviscid in the limit of vanishing radial distance with respect to the cowl edge.

The basic equations describing the Prandtl-Meyer expansion process are

$$p/\rho^{\Gamma} = \text{constant} \tag{44}$$

$$h + \frac{1}{2} V^2 = \text{constant} \tag{45}$$

$$\frac{dp}{\rho} + \frac{1}{2} d(V^2) = 0 \tag{46}$$

$$\frac{1}{\Gamma} d \ln(p) \pm d\theta = 0 \tag{47}$$

$$\Gamma = \Gamma (p, h, \Phi) \quad \text{where } \Phi = \text{constant} \tag{14}$$

For a small incremental step Δp, Equations (46), (47) 14) and (50) can be written

$$V_2^2 - V_1^2 = - \left(\frac{2\Gamma}{\Gamma-1}\right) \left[\left(\frac{p}{\rho}\right)_2 - \left(\frac{p}{\rho}\right)_1\right] \tag{48}$$

$$\frac{1}{\Gamma} \ln (p_2/p_1) \pm (\theta_2 - \theta_1) = 0 \tag{49}$$

$$p_2/\rho_2^{\Gamma} = p_1/\rho_1^{\Gamma} \tag{50}$$

where Γ is held constant in the integration step, yielding values for V_2, ρ_2 and θ_2. Then Equation (45) yields h_2. In this manner, the Prandtl-Meyer equations may be integrated, for a mixture in equilibrium.

Since the flow deflection and pressure downstream of the shock wave and Prandtl-Meyer are unknown an iteration process is required. A typical interaction calculation proceeds as follows. A shock wave angle is assumed for which flow properties (p, h, θ etc.) are computed downstream of the shock wave. Equations (44) through (47) are solved using small increments of Δp. The pressure behind the shock is the final pressure and the jet pressure is the initial pressure. If the turning angle for the expansion does not agree with the flow angle behind the shock to within a specified tolerance, a new shock wave angle is assumed and the process repeated until convergence is obtained.

After this solution is obtained, the program continues the normal calculation procedure until the last expansion ray is completed. The program terminates the calculation along the last ray. It is anticipated that the flow along the dividing streamline will not in general affect the pressure distribution along the undersurface, for the vehicles to be considered.

D. Over-expansion Phenomena - The nozzle over-expansion at the cowl is computed in a similar fashion to the under-expansion phenomena, except that a shock wave is required in the nozzle flow and an expansion in the external flow as depicted in Figure (8b). For purposes of simplicity

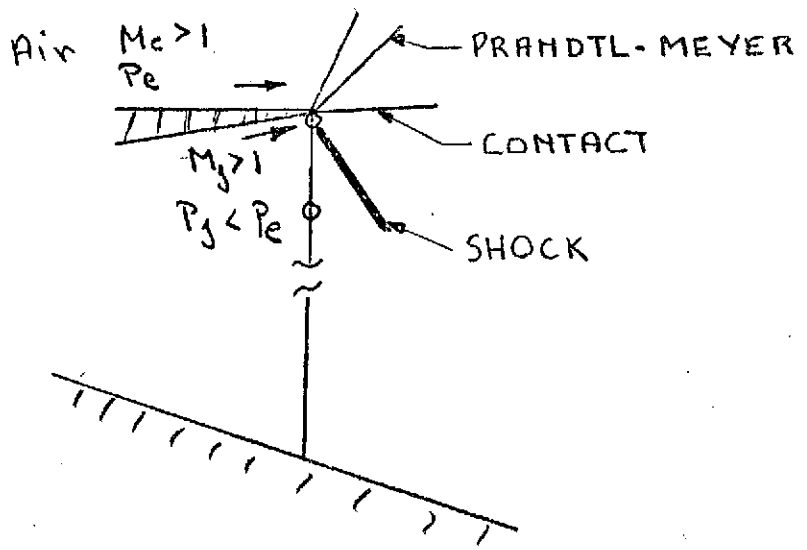

FIGURE 8b. OVER-EXPANSION INTERACTION

it is assumed that the external flow is initially uniform with constant ratio of specific heats. Further, it is assumed that pressure-flow deflection relationship on the external side of the dividing streamline is described by simple Prandtl-Meyer relations. These assumptions do not inhibit the programs generality, but are intended only to simplify the computation. They are readily removed and more general but complex methods can be used if the need arises.

Since the program stores data on C_- characteristics, shock waves of the C_+ family are conveniently traced. Thus, in order not to disrupt the program logic the problem is inverted so as to trace the over-expansion shock as a C_+ wave. This procedure is performed automatically as part of the program logic.

E. Contact Surface - A contact surface is a stream surface of the flow, therefore, the pressure and flow deflection must be continuous across the discontinuity. Figure (9) illustrates a contact surface calcula-

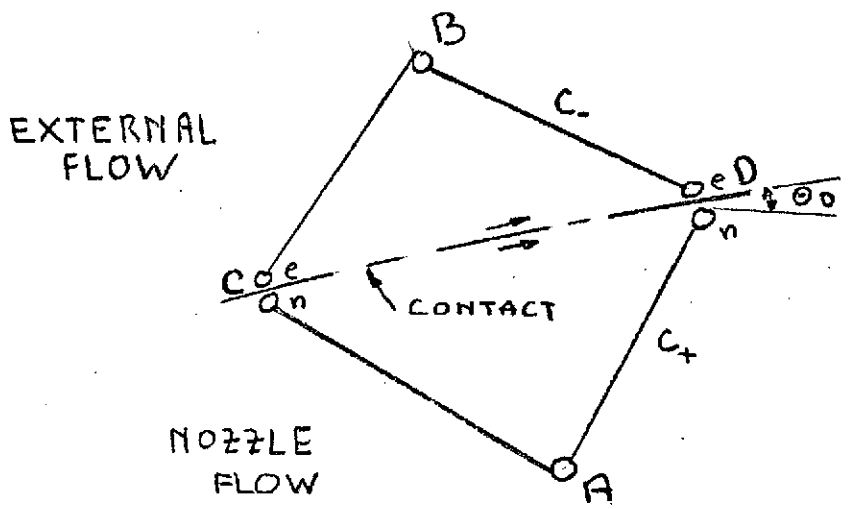

FIGURE 9. CONTACT CALCULATION

tion for supersonic flow. In the present program the characteristic on the external flow side is replaced by a Prandtl-Meyer pressure-flow deflection relation and the external flow is assumed uniform. The solution requires a iterative procedure similar to a wall boundary calculation except that the shape of the boundary (i.e., contact surface) is not known a priori.

In Figure (9) CD is the contact and point A lies on a C_- characteristic CA, on which all properties have previously been calculated. A guess is made for θ_D and for $\alpha = 1$ and $\beta = 0$ a simultaneous solution of the equations

$$\frac{y_D - y_C}{x_D - x_C} = \frac{1}{2}(\tan \theta_D + \tan \theta_C) = M_3 \tag{51}$$

and

$$\frac{y_D - y_A}{x_D - x_A} = M_{1_{nozzle}} \tag{18a}$$

yields XD and YD. Using the guessed value of θ_D from the characteristic relation along AC and the Prandtl-Meyer relation in the external stream two values of pressure are obtained at D. If these do not agree to within a specified tolerance a new guess for θ_D is made and the process repeated until convergence is achieved. Using the streamline relations along CD the remaining properties (q, h, T etc.) are computed on each side of the discontinuity and the process repeated for $\alpha = \frac{1}{2}$, $\beta = \frac{1}{2}$.

F. Shock Reflection At Wall - The incident and reflected strength of a shock wave at a wall boundary is determined by the condition that downstream of the reflected wave (3) the flow deflection at the wall must equal the wall slope; Figure (10) depicts this interaction.

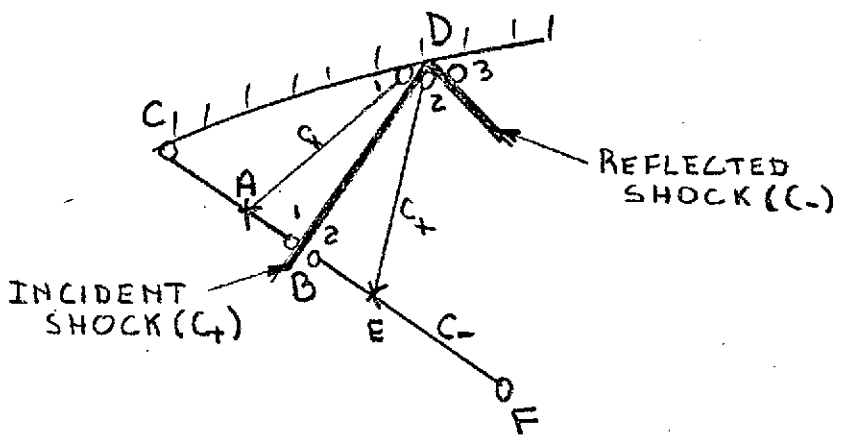

FIGURE 10. SHOCK REFLECTION AT WALL

The solution requires an iterative procedure since the reflected wave strength is a function of the data downstream of the incident wave (2) and subject to the above constraint. A shock angle sigma (σ_1) is assumed for the incident wave and the location of the shock wall intersection (x_D, y_D) is computed using

$$\frac{y_D-y_A}{x_D-x_A} = \frac{1}{2}(\tan \sigma_{D_1} + \tan \sigma_B) = M_3$$

and

$$y_D = A_j (x_D-x_i)^2 + B_j (x_D-x_i) + C_j$$

which yields (x_D, y_D, θ_D).

Since the flow upstream of the shock wave is nonuniform, a characteristic solution similar to a wall calculation is required to determine the flow properties at D_1. Note that point A is interpolated on the C_- characteristic CB_1. Then the Hugoniot relations Equations (38) through (43) yield the flow properties downstream of the incident wave (2). The pressure from this calculation is then compared with a characteristic calculation along ED_2 on the downstream side. Point E is interpolated on C_- characteristic B_2F. If the pressures do not agree to within a specified tolerance, a new shock angle is assumed and the process repeated until convergence.

These properties are then used as upstream conditions for the reflected wave. Assuming a reflected wave angle sigma (σ_3) the Hugoniot relations yield the flow properties downstream. If the flow angle does not agree with the wall angle to within a specified tolerance a new reflected wave angle is assumed and the process repeated until convergence. After convergence the entire calculation is repeated with $\alpha = \frac{1}{2}$ and $\beta = \frac{1}{2}$.

Since the program logic stores data only on C_- characteristics, shock waves of the C_+ family are conveniently traced. However, the reflected wave is a C_- wave as depicted in Figures (3) and (10). In order not to disrupt the program logic, after computing the strength of the reflected wave the flow

field is automatically inverted making the reflected wave a C_+ shock wave. Special provisions are required, however, for storing new initial data along a line which enables the propagation strength of the reflected wave to be computed up to the next boundary. The program logic is such that these requirements are performed automatically. The overall grid for this calculation is shown in Figure (3) of Section IIC.

IV. SAMPLE CALCULATIONS

Figure (11) depicts an under-expanded nozzle calculation using NASA supplied geometry and initial conditions. The upper curves represent a comparison of vehicle undersurface pressures between two dimensional NASA calculations and the subject ATL program. Excellent agreement is seen to exist over the length of the undersurface.

The lower curve in Figure (11) represents a nozzle with the same geometry and initial conditions except that a lateral nozzle area variation has been provided for between the throat surface and the cowl. The origin of the source is at $x/h_t = 7$. Downstream of the cowl the flow is assumed to be two dimensional. The lateral area variation is seen to produce significant changes in the pressure distribution on the undersurface and in the location and strength of waves. Thus, this approximation to the lateral area variation can be a powerful tool in the design of scramjet nozzle exhaust flow fields.

Figures (12) and (13) demonstrates the programs capability to calculate over-expanded nozzle flows. Figure (12) is a trace of the vehicle geometry, shock shape and contact shape upto $x/h_t = 27$. Figure (13) indicates the pressure distributions on the cowl - contact surface and the vehicle undersurface for this case. The under-expansion shock jump is clearly visible at the cowl trailing edge ($x/h_t = 6$).

TABLE I

UNDER-EXPANDED FLOW

A. Case Ia - Two Dimensional

Initial Conditions

Temperature (T/T_∞) - 10.1
Pressure (p/p_∞) - 36.65
Velocity (q/u_∞) - 0.929
Mach Number M - 2.91
Flow Angle θ - 0.
Equivalence Ratio Φ - 1.0
Source origin - none, two dimensional

Free Stream Conditions

Altitude - 101,800 ft.
Mach Number M_∞ - 10.
Pressure p_∞ - 23.09 lb/ft^2
Temperature T_∞ - 418.8°R

External Flow

Temperature (T/T_∞) - 1.0
Pressure (p/p_∞) - 1.0
Velocity (q/u_∞) - 1.0
Mach Number M - 10.
Flow Angle θ - 0.
Equivalence Ratio Φ - 0.

Geometry - $Y=AX^2+BX+C$

	Vehicle			Cowl	
X	0 - .4	.4 - 8.0	8.0 - End.	0 - .4	.4 - 3.0
A	-.5565	0	.01019	.1314	0
B	0	-.4452	-.6082	0	.1051
C	0	.08905	.7410	1.0	.9790

B. Case Ib - Source Flow

All data is the same as Case (Ia) except initial source origin is located at x = -7.0.

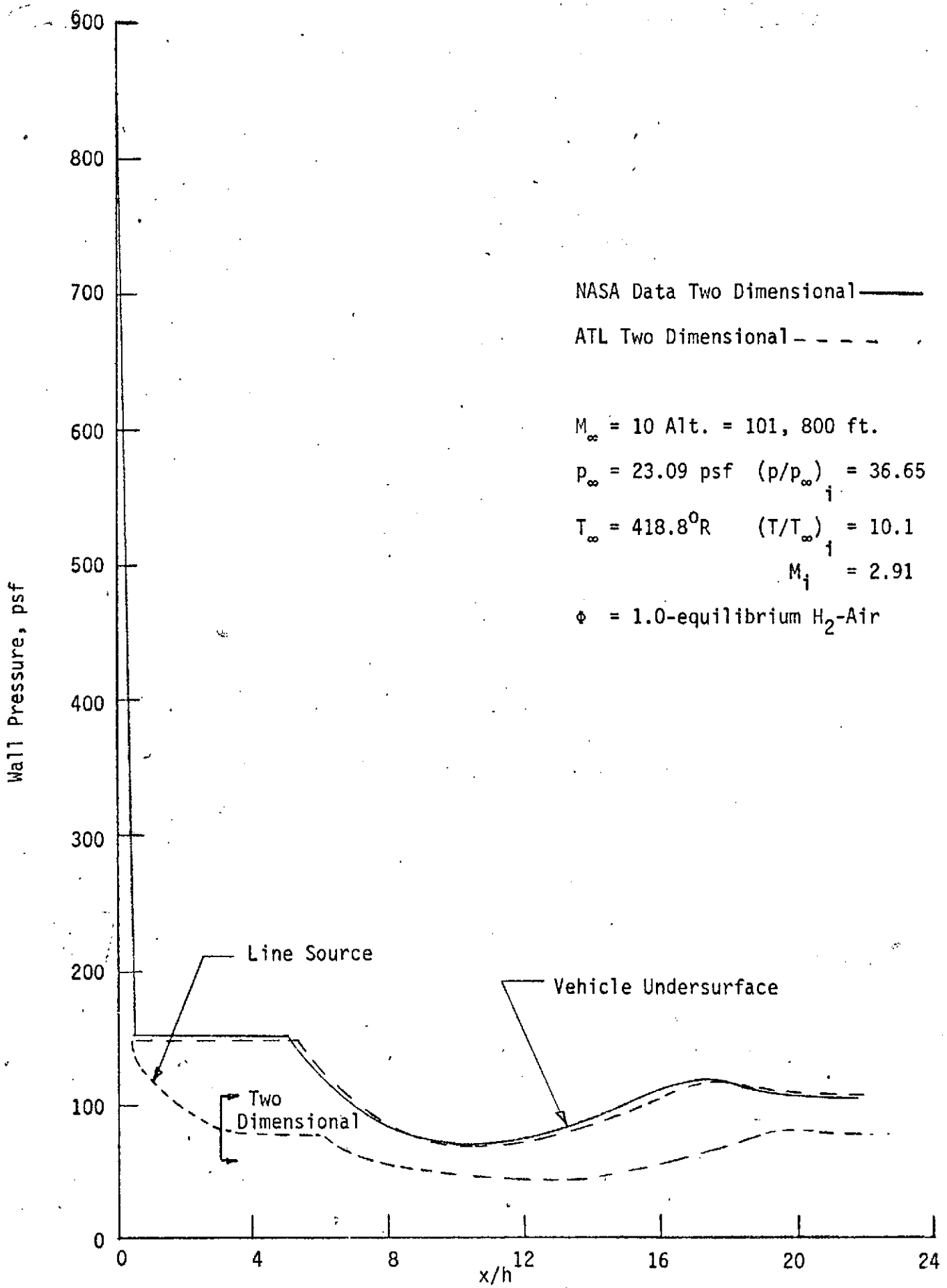

FIGURE 11. VEHICLE UNDER-EXPANDED PRESSURE DISTRIBUTION

TABLE II

OVER-EXPANDED FLOW

Case II - Two Dimensional

Initial Conditions

Temperature	(T/T_∞)	- 10.77
Pressure	(p/p_∞)	- 20.55
Velocity	(q/u_∞)	- .904
Mach Number	M	- 1.09
Flow Angle	θ	- 0.
Equivalence Ratio	Φ	- 0.

Source origin - none, two dimensional

Free Stream Conditions

Altitude	- 60,000 ft.
Mach Number	- 4.0
Pressure p_∞	- 151 lbs/ft^2
Temperature T_∞	- 390°R

External Flow

Temperature	(T/T_∞)	- 1.327
Pressure	(p/p_∞)	- 2.493
Velocity	(q/u_∞)	- .95
Mach Number	M	- 6.67
Flow Angle	θ	- 0.
Equivalence Ratio	Φ	- 0.

Geometry - $Y=AX^2+BX+C$

	Vehicle			Cowl	
X	0 - .4	.4 - 8.0	8.0 - End	0 - . 4	.4 - 6.0
A	-.5565	0	.01019	.3117	0
B	0	-.4452	-.6082	0	.2493
C	0	.08905	.7410	1.0	.9501

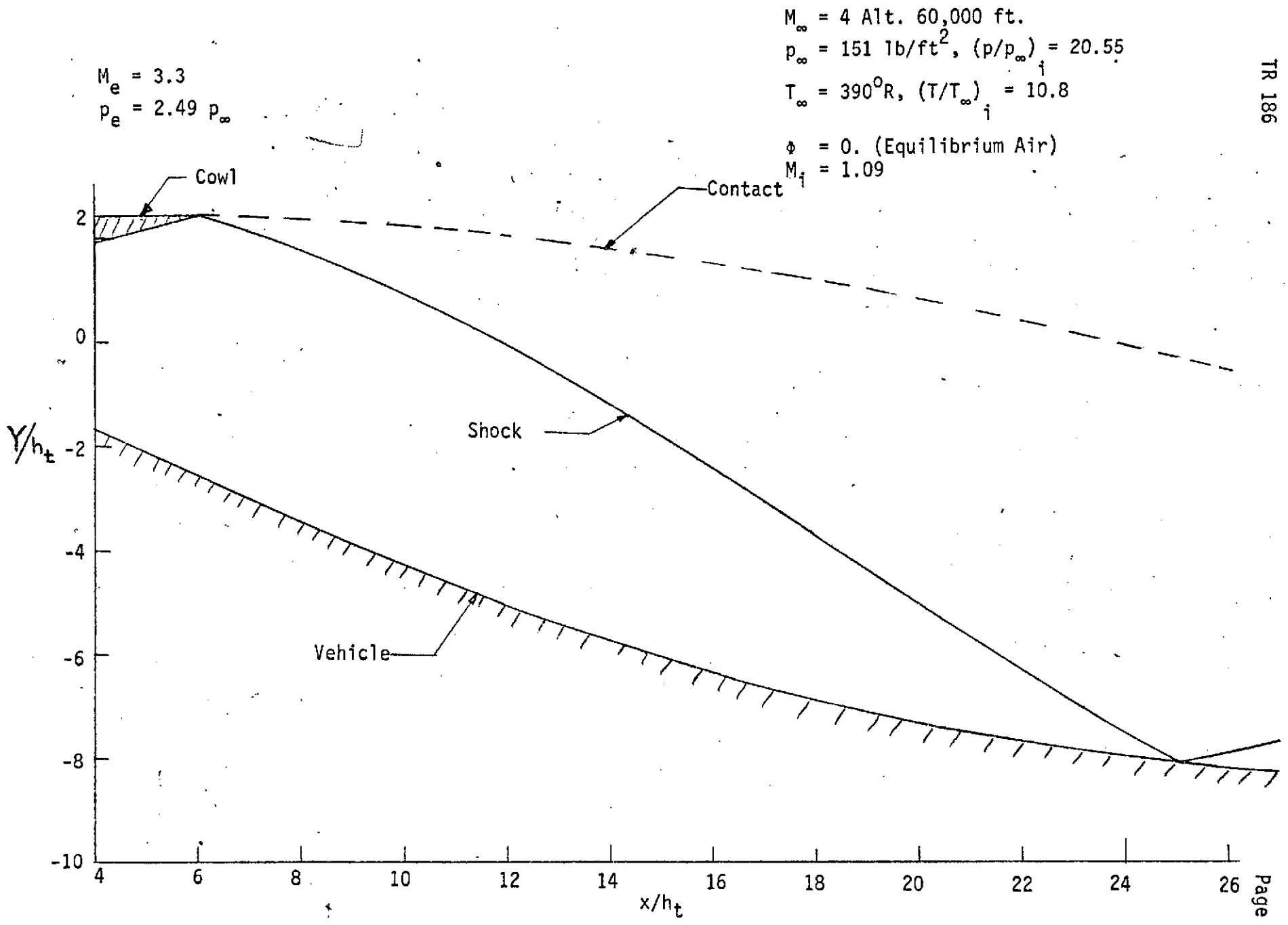

FIGURE 12. OVER-EXPANDED SHOCK AND CONTACT

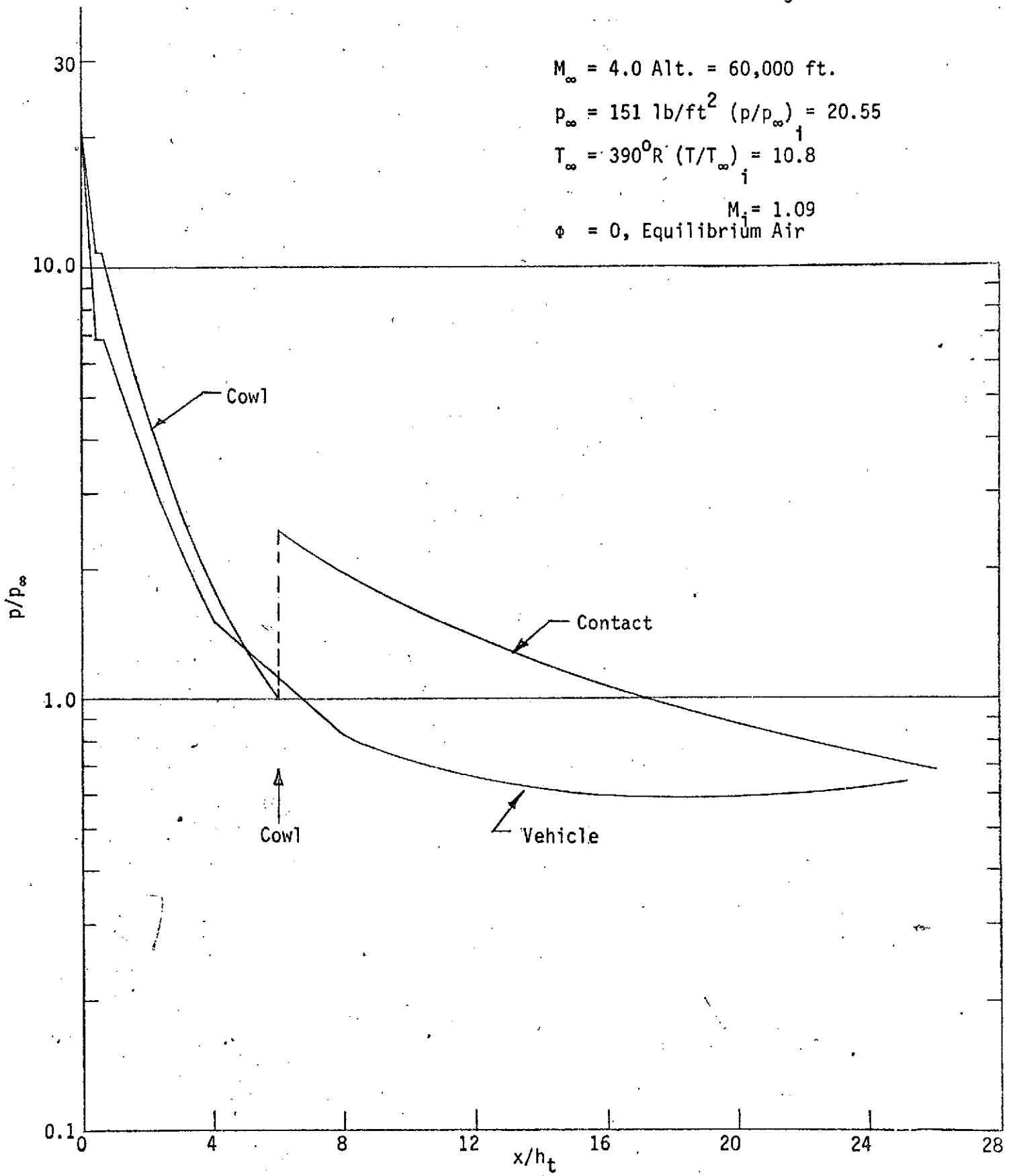

FIGURE 13. TWO DIMENSIONAL OVER-EXPANDED FLOW

V. CONCLUSIONS

A unique characteristic procedure has been developed which computes realistic scramjet nozzle exhaust flow fields. The use of an axially expanding coordinate system (line source) allows lateral nozzle area variations to be accounted for in a quasi two dimensional fashion. Additional geometric flexibility is incorporated in the numerical procedure through the use of additional coordinate systems i.e., axisymmetric, and Cartesian.

The numerical procedure uses a free running characteristic grid, but stores data on the C_- characteristics. The technique is second order accurate in the characteristic sense.

The wide variety of boundary conditions incorporated into the program permits the calculation of wall boundaries, shock boundaries, contact boundaries, shock-wall intersections and over or under-expansion interactions.

The use of the unique hydrogen-air equilibrium curve fits developed in Reference (5), as well as frozen hydrogen-air chemistry permits bounding the complex chemical phenomena which occur in exhaust nozzle flows.

Thus, it is felt that the current program will give the designer of scramjet nozzle exhaust flow fields a flexibility not available with previous methods.

REFERENCES

1. Ferri, A., "Analysis and Design of Three Dimensional Supersonic Nozzles -- A Design Technique for Multiple Nozzle Configurations," ATL TR 166, Volume III, October 1972.

2. Ferri, A. and Del Guidice, P., "A Design Technique for Multiple Nozzle Configurations," ATL TM 174, May 1973.

3. Ferri, A., "Methodology for Three Dimensional Nozzle Design," ATL TM 176, August 1973.

4. McBride, B. J., Heimel, J., Ehlers, S. G. and Gordon, S., "Thermodynamic Properties to 6000^{0}K for 210 Substances Involving the First 18 Elements," NASA SP-3001 (1963).

5. Dash, S. and Del Guidice, P., "Analysis and Design of Three Dimensional Supersonic Nozzles -- Nozzle Exhaust Flow Field Analysis by a Reference Plane Characteristic Technique," ATL TR 166, Volume I, October 1972.

6. Dash, S., "The Determination of Nozzle Contours for Rotational, Non-Homentropic Gas Mixtures," ATL TR 148, March 1970.

7. Kalben, P. and Del Guidice, P., "FORTRAN Program Manual for Source Flow Characteristics Procedure," ATL TM 179, March 1974.

APPENDIX I

CHARACTERISTIC DERIVATION
FROZEN FLOW

The continuity equation (Equation (1)) may be expanding yielding:

$$\rho \frac{\partial q}{\partial s} + q \frac{\partial \rho}{\partial s} + \rho q \frac{\partial \theta}{\partial n} + J \frac{\rho q}{y} \sin \theta + J_2 \frac{\rho q}{x} \cos \theta = 0 \qquad (I.1)$$

From the s-momentum equation

$$\rho \frac{\partial q}{\partial s} = - \frac{1}{q} \frac{\partial p}{\partial s}$$

and using both the Equation of State (6) and the energy Equation (4), the term $\frac{\partial \rho}{\partial s}$ may be replaced by

$$\frac{\partial \rho}{\partial s} = \left(\frac{W \gamma_\infty}{T W_\infty} M_\infty^2 - \frac{(\gamma_\infty - 1)}{C_p T} M_\infty^2 \right) \frac{\partial p}{\partial s}$$

Making these substitutions in Equation (I.1), and multiplying through by q, we obtain

$$\left(\frac{q^2}{T} \left(\frac{W \gamma_\infty}{W_\infty} M_\infty^2 - \frac{(\gamma_\infty - 1)}{C_p} M_\infty^2 \right) - 1 \right) \frac{\partial p}{\partial s} + \rho q^2 \frac{\partial \theta}{\partial n} \qquad (I.2)$$

$$+ \frac{J \rho}{y} q^2 \sin \theta + J_2 \frac{\rho q^2}{x} \cos \theta = 0$$

By algebraic manipulation, using Equations (11) and (12), the

APPENDIX I (Continued)

term multiplying $\frac{\partial p}{\partial s}$ in (I.2) may be reduced to (M^2-1) and hence Equation (I.2) becomes

$$\frac{(M^2-1)}{\rho q^2}\frac{\partial p}{\partial s} + \frac{\partial \theta}{\partial n} + \frac{J_1}{y}\sin\theta + \frac{J_2}{x}\cos\theta = 0 \qquad (I.3)$$

Using Equations (11) and (14) $\rho q^2 = \gamma p M^2$. Making this substitution in both Equations (I.3) and the normal momentum equation, we obtain

$$\frac{(M^2-1)}{\gamma p M^2}\frac{\partial p}{\partial s} + \frac{\partial \theta}{\partial n} = -\frac{J_1}{y}\sin\theta - \frac{J_2}{x}\cos\theta \qquad (I.4)$$

$$\frac{1}{\gamma p M^2}\frac{\partial p}{\partial n} + \frac{\partial \theta}{\partial s} = 0 \qquad (I.5)$$

The total derivatives of p and θ may be expressed by:

$$\frac{\partial p}{\partial s}\,ds + \frac{\partial p}{\partial n}\,dn = dp \qquad (I.6)$$

$$\frac{\partial \theta}{\partial s}\,ds + \frac{\partial \theta}{\partial n}\,dn = d\theta \qquad (I.7)$$

Written in matrix form, the above system (Equations (I.4) through (I.7)) becomes

APPENDIX I (Continued)

$$\begin{pmatrix} (M^2-1)/\gamma pM^2 & 0 & 0 & 1 \\ 0 & 1/\gamma M^2 p & 1 & 0 \\ ds & dn & 0 & 0 \\ 0 & 0 & ds & dn \end{pmatrix} \begin{pmatrix} \frac{\partial p}{\partial s} \\ \frac{\partial p}{\partial n} \\ \frac{\partial \theta}{\partial s} \\ \frac{\partial \theta}{\partial n} \end{pmatrix} = \begin{pmatrix} -\left(\frac{J_1}{y}\sin\theta + \frac{J_2}{x}\cos\theta\right) \\ 0 \\ dp \\ d\theta \end{pmatrix} \qquad (I.8)$$

The characteristic directions of this system of equations are obtained by setting the determinant of the coefficient matrix equal to zero,

$$\begin{vmatrix} (M^2-1)/\gamma M^2 p & 0 & 0 & 1 \\ 0 & 1/\gamma M^2 p & 1 & 0 \\ ds & dn & 0 & 0 \\ 0 & 0 & ds & dn \end{vmatrix} = 0 \qquad (I.9)$$

obtaining $\frac{dn^2}{ds} = \frac{1}{(M^2-1)}$. Hence the characteristics are lines whose slope is given by

$$\frac{dn}{ds} = \pm \frac{1}{\sqrt{M^2-1}} = \tan\mu \tag{I.10}$$

or expressed in Cartesian coordinates

$$\frac{dy}{dx} = \tan(\theta \pm \mu) \tag{I.11}$$

The compatibility relation along the characteristics is obtained by replacing any column of the coefficient matrix with the vector on the right-hand side of Equation (I.8) and setting the determinant of this matrix equal to zero.

$$\begin{vmatrix} -\left(\frac{J_1 \sin\theta}{y} + \frac{J_2}{x}\cos\theta\right) & 0 & 0 & 1 \\ 0 & \frac{1}{\gamma M^2 p} & 1 & 0 \\ dp & dn & 0 & 0 \\ d\theta & 0 & ds & dn \end{vmatrix} = 0 \tag{I.12}$$

Expanding the determinant and using Equation (I.10) we obtain the compatibility relation (Equation 8).

$$\frac{\sin\mu \cos\mu}{\gamma} d \ln p \pm d\theta + \left(\frac{J_1 \sin\theta}{y} + \frac{J_2 \cos\theta}{x}\right) \frac{\sin\mu}{(\cos\theta \pm \mu)} dx = 0 \tag{I.13}$$

Since we may write total derivatives for the changes in entropy, stagnation enthalpy and species mass fraction along streamlines, the streamlines act as characteristics in the flow field. Hence, along a streamline, whose slope is given by

$$\frac{dy}{dx} = \tan\theta \tag{I.14}$$

the following equations hold:

$$dS = 0 \tag{I.15}$$

$$dH = 0 \tag{I.16}$$

and

$$d\alpha_i = 0 \tag{I.17a}$$

For a flow in chemical equilibrium the derivation is identical with the frozen ratio of specific heats γ replaced by Γ and the Mach number defined in terms of the local equilibrium sound speed. Equation (I.17a) is replaced by

$$d\Phi = 0. \tag{I.17b}$$

APPENDIX IIa

THERMODYNAMIC COEFFICIENTS FOR FROZEN SPECIES

The following thermodynamic properties have been tabulated as polynomials in temperature (in degrees Kelvin) in the form below:

$$\frac{C^*_{p_i}}{R_o} = a_1 + a_2 T^* + a_3 T^{*2} + a_4 T^{*3} + a_5 T^{*4} \qquad \text{(IIa.1)}$$

$$\frac{h^*_i}{R_o T^*} = a_1 + \frac{a_2}{2} T^* + \frac{a_3}{3} T^{*2} + \frac{a_4}{4} T^{*3} + \frac{a_5}{5} T^{*4} + \frac{a_6}{T^*} \qquad \text{(IIa.2)}$$

$$\frac{S^*_i}{R_o} = a_1 \ln T^* + a_2 T^* + \frac{a_3}{2} T^{*2} + \frac{a_4}{3} T^{*3} + \frac{a_5}{4} T^{*4} + a_7 \qquad \text{(IIa.3)}$$

The coeffients ($a_1 - a_7$) have been tabulated for the temperature intervals 300° to 1000°k and 1000° to 5000°k in Reference (4).

APPENDIX IIb

EQUILIBRIUM HYDROGEN-AIR

CURVE FITS FOR Γ, h and ρ

The variation of Γ (the equilibrium value of γ) as a function of temperature (T), pressure (P) and equivalence ratio (Φ) is presented graphically in Figures (A1), (A2) and (A3) from values tabulated in Reference (4). In Figure (A1) it can be seen that Γ is a strong function of T over the temperature range of interest, while the effect of varying composition is small by comparison. Moreover, Figure (A2) indicates that Γ is moderately sensitive to pressure and the degree of sensitivity increases substantially as the temperature level increases and dissociation effects become important.

As a result of these observations, temperature is the primary independent variable, while pressure is the secondary independent variable and composition acts as a perturbation variable. Thus, we can fit the function Γ (T,P,Φ) with a polynomial in T and add on a temperature dependent correction term for the effect of pressure and a temperature independent correction term for the effect of Φ.

An examination of Figure (A1) suggest that the function Γ (T) can best be curve fit by breaking up the temperature range into three intervals such that the function can be represent-

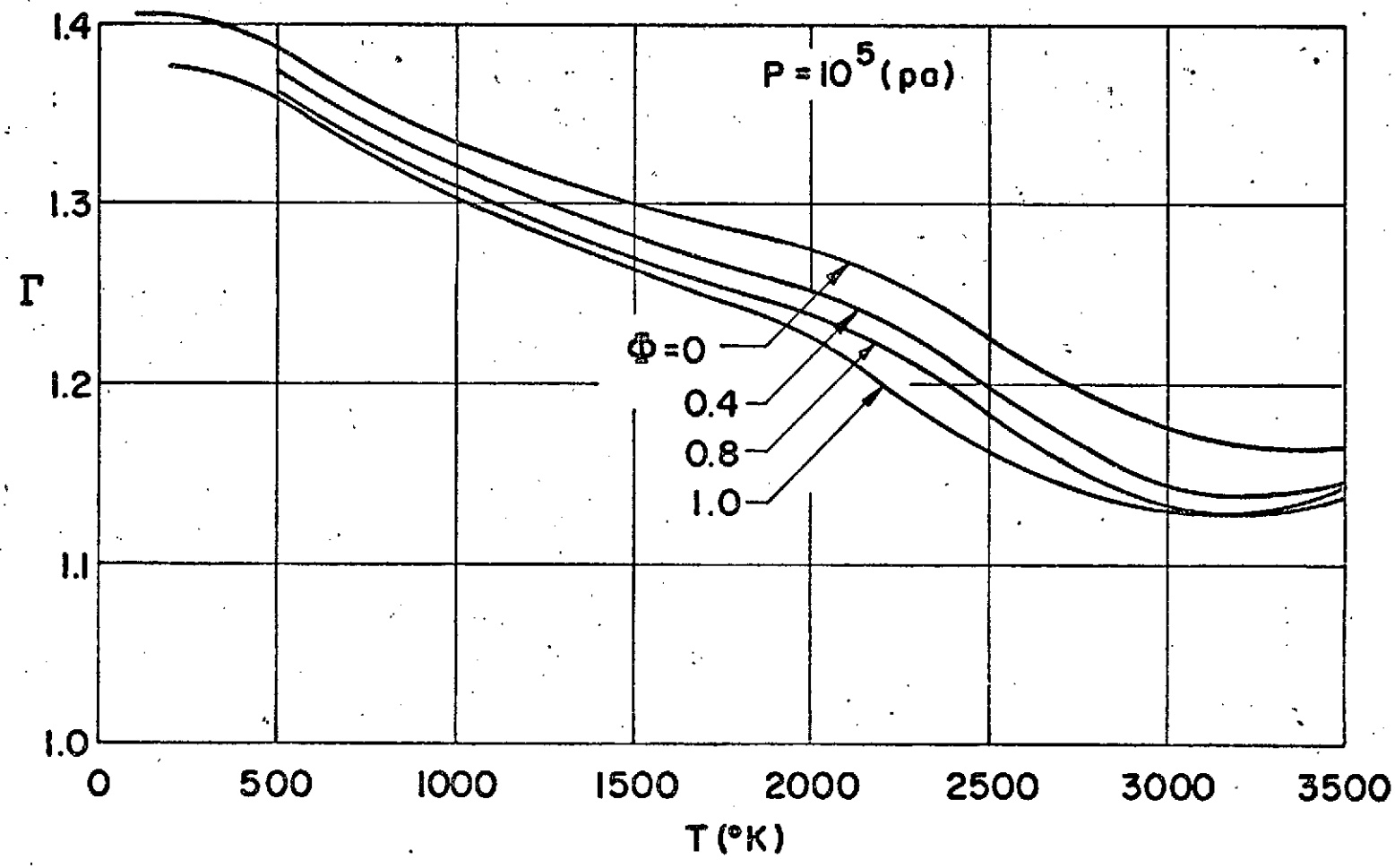

FIGURE A1. Γ VARIATION WITH TEMPERATURE

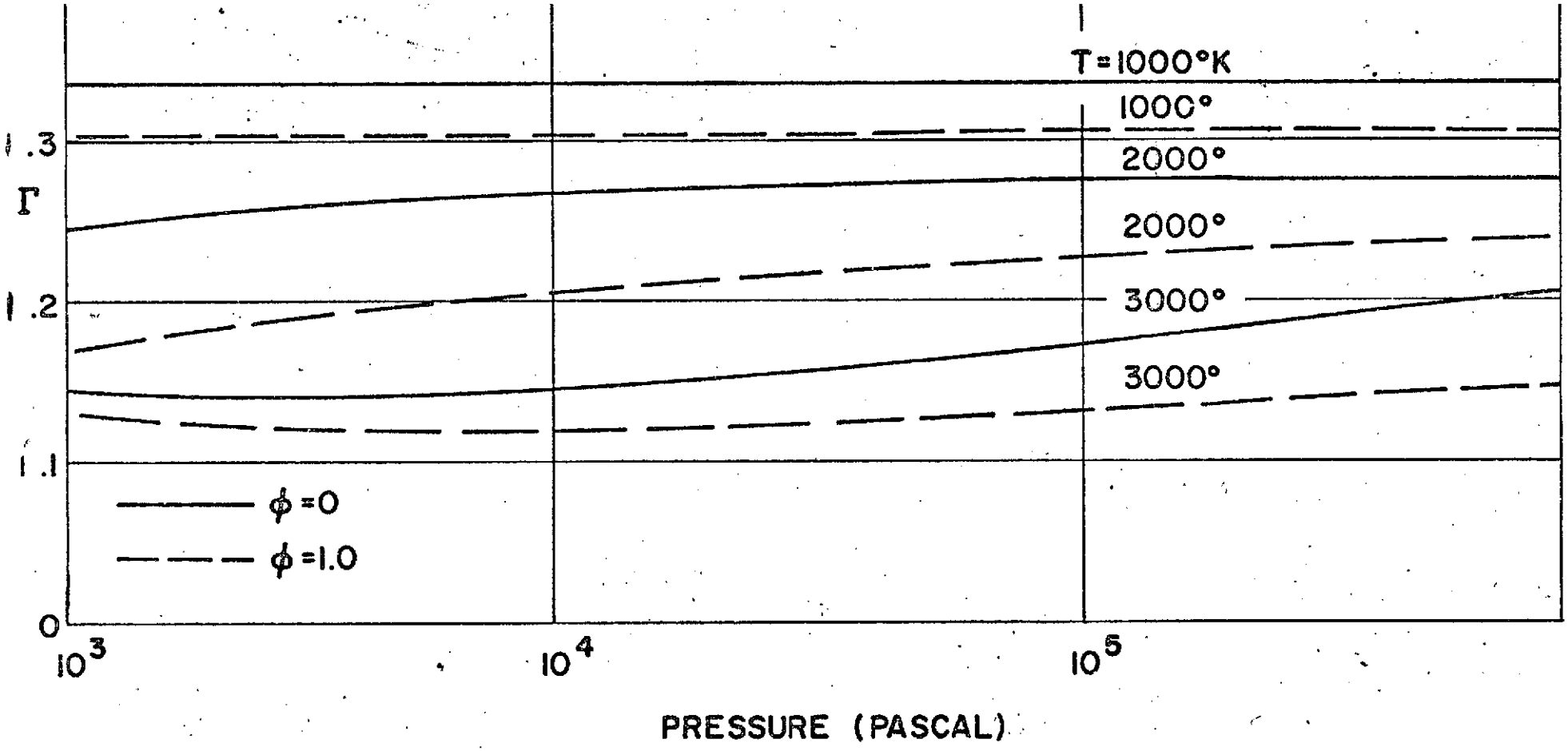

FIGURE A2. Γ VARIATION WITH PRESSURE

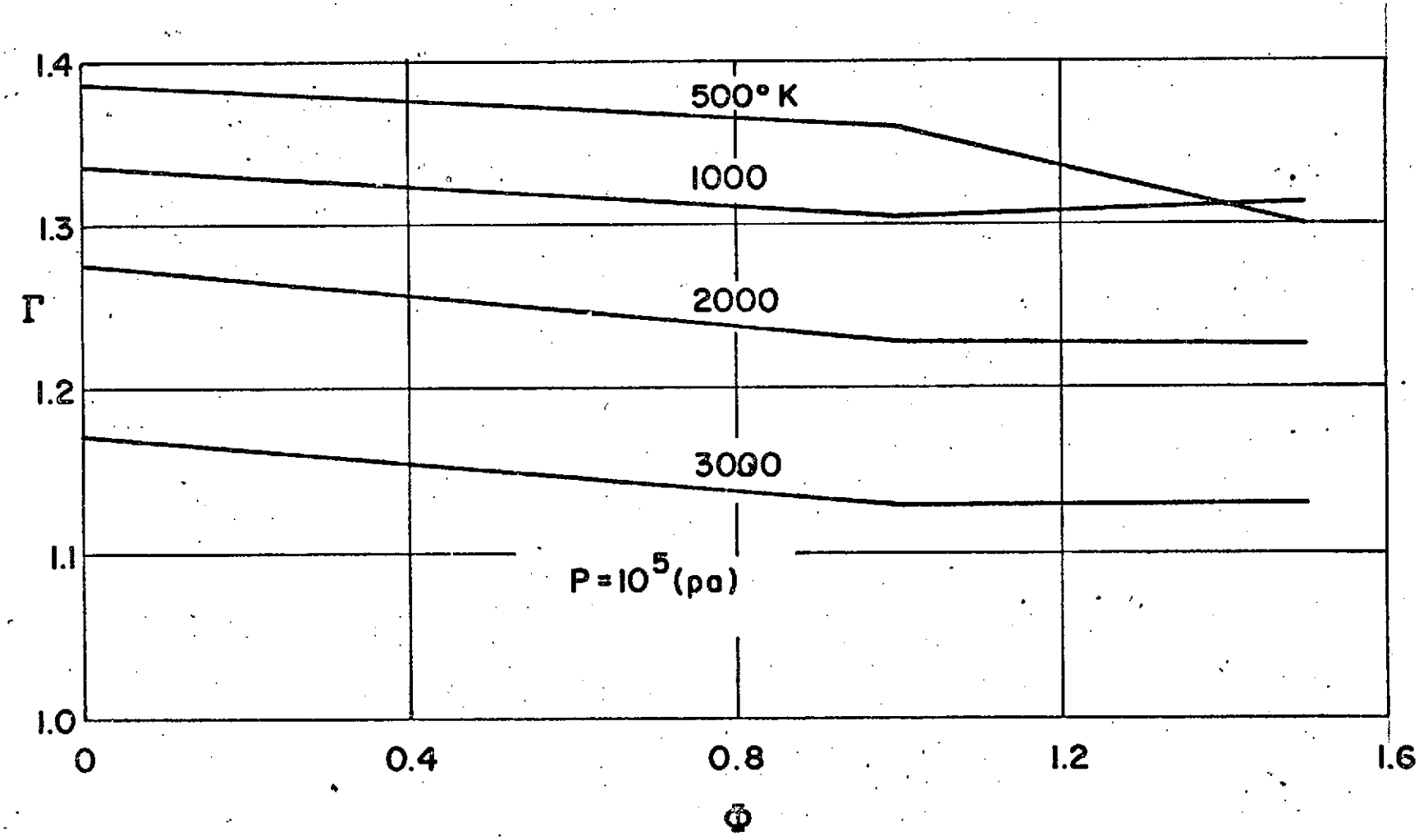

FIGURE A3. Γ VARIATION WITH Φ

ed by a parabola in each range. Choosing $p = 10^5$ pascal and $\phi=1$ as our base, we therefore find three functions

$$\Gamma_1(T,10^5,1) = - 1.833\times10^{-7}\ T^2 + 7.5\times10^{-5}\ T + 1.367 \qquad \text{(IIb.1)}$$

$$\Gamma_2(T,10^5,1) = 2.0\times10^{-8}\ T^2 - 1.38\times10^{-4}\ T + 1.423 \qquad \text{(IIb.2)}$$

$$\Gamma_3(T,10^5,1) = 7.27\times10^{-8}\ T^2 - 4.57\times10^{-4}\ T + 1.85 \qquad \text{(IIb.3)}$$

and define the basic temperature function as

$$\Gamma(T,10^5,1) = \left\{\begin{matrix}\Gamma_1(T,10^5,1)\\ \Gamma_2(T,10^5,1)\\ \Gamma_3(T,10^5,1)\end{matrix}\right\} \text{ for } \left\{\begin{matrix}T\leq 500^oK\\ 500\leq T\leq 2000^oK\\ T\geq 2000^oK\end{matrix}\right\} \qquad \text{(IIb.4)}$$

Figure (A3) indicates that $\frac{\partial\Gamma}{\partial\Phi}$ is constant in the two ranges $\Phi<1$ and $\Phi>1$, but is a function of T. Fitting the function $\frac{\partial\Gamma}{\partial\Phi}$ in each of the ranges of ϕ we obtain

$$\frac{\partial\Gamma}{\partial\Phi} = \begin{bmatrix}n_1(T)\\ n_2(T)\end{bmatrix} \text{ for } \begin{bmatrix}\Phi\leq 1\\ \Phi\geq 1\end{bmatrix} \qquad \text{(IIb.5)}$$

where

$$n_1(T) = 4\times10^{-9}\ T^2 - 2\times10^{-5}\ T - 0.019 \qquad \text{(IIb.6)}$$

$$n_2(T) = 3.39\times10^{-2}\ T^{0.5} - 3.91\times10^{-4}\ T - 0.681 \qquad \text{(IIb.7)}$$

This now defines Γ as a function of both temperature and Φ by means of the equation

$$\Gamma(T,10^5,\Phi) = \Gamma(T,10^5,1) + (\Phi-1)\frac{\partial\Gamma}{\partial\Phi} \qquad \text{(IIb.8)}$$

Finally, the effect of pressure must be included. From Figure (18) we observe that Γ may be approximated as

$$\Gamma(T,P,\Phi) = \Gamma(T,10^5,\Phi) + m\,[\log_{10}(p) - 5] \qquad \text{(IIb.9)}$$

where m is a function of T. Deriving m, we find

$$m = \left\{ \begin{array}{l} 0 \\ -2.15\times10^{-8}T^2+0.91\times10^{-4}T-0.0695 \end{array} \right\} \text{ for } \left\{ \begin{array}{l} T<1000^{\circ}K \\ T\geq1000^{\circ}K \end{array} \right\} \qquad \text{(IIb.10)}$$

Summarizing, the final function obtained is

$$\Gamma(T,P,\Phi) = \Gamma(T,10^5,1) + m\left(\frac{\ln p}{2.3} - 5\right) + \frac{\partial\Gamma}{\partial\Phi}(\Phi-1)$$

where the functions $\Gamma(T,10^5,1)$, $\frac{\partial\Gamma}{\partial\Phi}$ and m are given by Equations (4), (5) and (10) respectively.

The curve fit for enthalpy is derived in a similar way. Figures (A-4) and (A-5) present the variation of h with temperature, pressure and equivalence ratio. As was the case for Γ, the

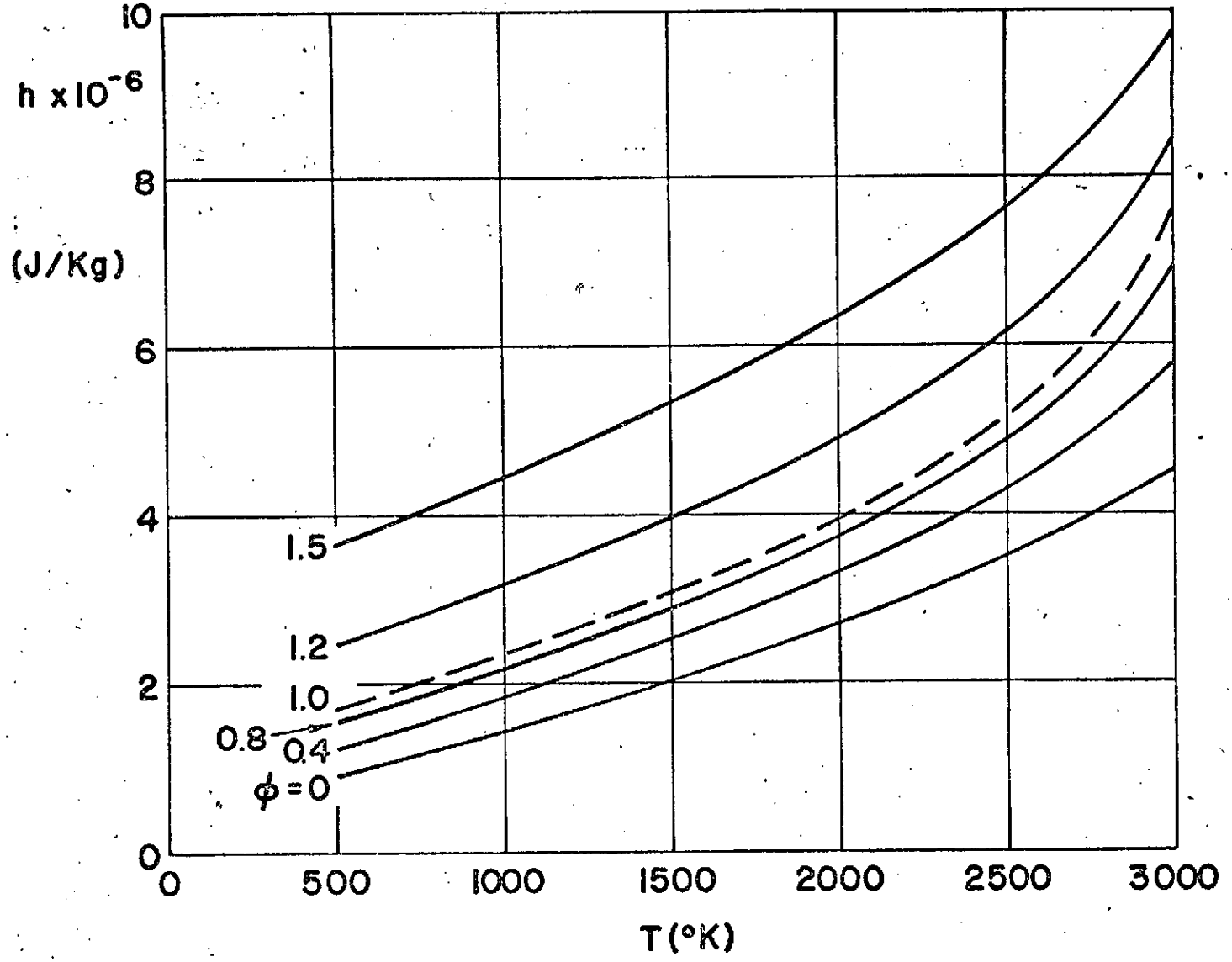

FIGURE A4. ENTHALPY AS A FUNCTION OF TEMPERATURE ($p=10^5$pa.)

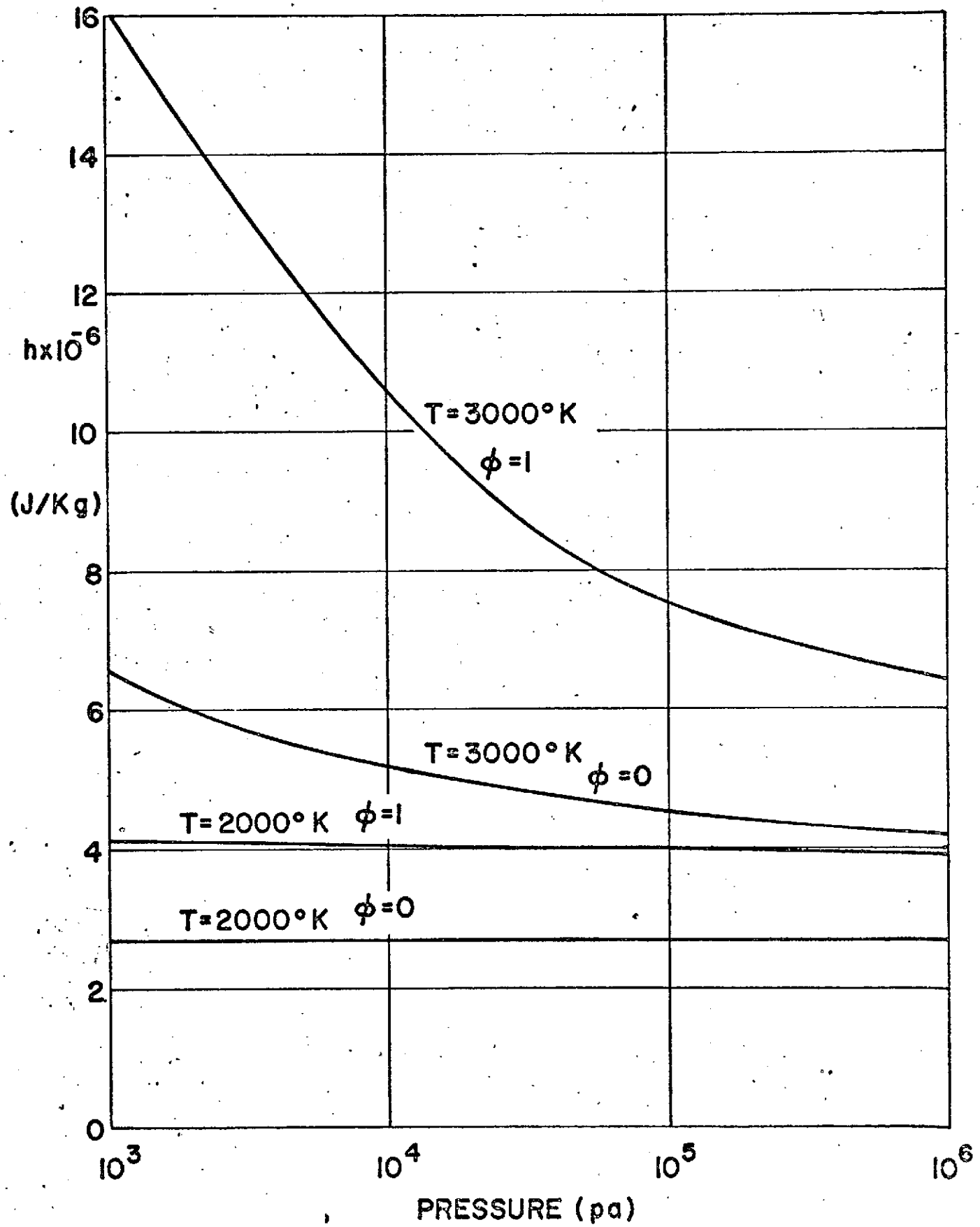

FIGURE A5. ENTHALPY AS A FUNCTION OF PRESSURE.

function $h(T, \phi, p)$ is fit by a quadratic function of T, the coefficients of which are functions of ϕ and an additive term for the effects of pressure. The resulting curve fit is summarized below.

$$h(T,\phi,p) = \begin{Bmatrix} h(T,\phi,10^5) \\ h(T,\phi,p) \end{Bmatrix} \quad \text{for} \quad \begin{Bmatrix} T \leq 2000^{\circ}K \\ T > 2000^{\circ}K \end{Bmatrix} \tag{IIb.11}$$

where $$h(T,\phi,p) = h(T,\phi,10^5)\ 1 + \left[\frac{(1+\phi)(T-2000)}{2000}\left(.125\left(\frac{\ln p}{2.3}-5\right)^2 - .275\left(\frac{\ln p}{2.3}-5\right)\right)\right] \tag{IIb.12}$$

The basic function $h(T,\phi,10^5)$ is defined as

$$h(T,\phi,10^5) = 10^6\ (a_1T^2+b_1T+c_1) \tag{IIb.13}$$

with the coefficients a_1, b_1 and c_1 defined below:

For $T \leq 2000^{\circ}K$ and $\phi \leq 1$ (IIb.14)

$$a_1 = 10^{-7}\ (-.1042\phi^2 + .8242\phi + .987)$$

$$b_1 = 10^{-3}\ (.01167\phi^2 + .1503\phi + .938) \tag{IIb.15}$$

$$c_1 = -.0284\phi^2 + .6731\ \phi + .4293$$

For $T \leq 2000^{o}K$ and $\phi \geq 1$

$$a_1 = 10^{-7} (1.787\phi^2 - 5.48\phi + 5.4)$$

$$b_1 = 10^{-3} (-.1867\phi^2 + 1.11\phi + .176) \qquad \text{(IIb.16)}$$

$$c_1 = -.0933\phi^2 + 3.975\phi - 2.808$$

For $T > 2000^{o}K$ and $\phi \leq 1$

$$a_1 = 10^{-6} (1.792\phi^2 + .3983\phi + .310)$$

$$b_1 = 10^{-3} (-9.05\phi^2 - .07917\phi + .245) \qquad \text{(IIb.17)}$$

$$c_1 = 10.86\phi^2 - .1183\phi + .970$$

For $T > 2000^{o}K$ and $\phi > 1$

$$a_1 = 10^{-6} (4.81\phi^2 - 13.9\phi + 11.59)$$

$$b_1 = 10^{-3} (-23.08\phi^2 + 66.82\phi - 52.61) \qquad \text{(IIb.18)}$$

$$c_1 = 27.05\phi^2 - 73.73\phi + 58.39$$

When the inverse function $T(h,\phi,p)$ is required, it is obtained by an iterative solution of Equations (12) through (18)

The density is found by obtaining a curve fit for the mixture molecular weight and using the equation of state

$$\rho = \frac{pm}{\bar{R}T} \tag{IIb.19}$$

where $\bar{R}$ is the universal gas constant and m is the molecular weight.

The behavior of m with T,p and ϕ is illustrated in Figures (A6) and (A7). We see that for temperatures less than 2000°K, m is essentially independent of temperature. The discontinuity in slope of $m(\phi)$ shown in Figure (A7) requires that the equivalence ratio range be split in two. Thus,

for $T \leq 2000^{\circ}K$

$$m(\phi) = \left\{ \begin{array}{l} 1.53\phi^2 - 5.895\phi + 28.965 \\ 1.60\phi^2 - 10.6\phi + 33.6 \end{array} \right\} \text{ for } \left\{ \begin{array}{l} \phi \leq 1 \\ \phi > 1 \end{array} \right\} \tag{IIb.20}$$

For the higher temperature range, it is convenient to employ the form

$$m = m(\phi) - \delta(p,\phi,T) \tag{IIb.21}$$

where

$$\delta = d_2(p,\phi) \left(\frac{T-2000}{1000}\right)^{n_2(\phi)} \tag{IIb.22}$$

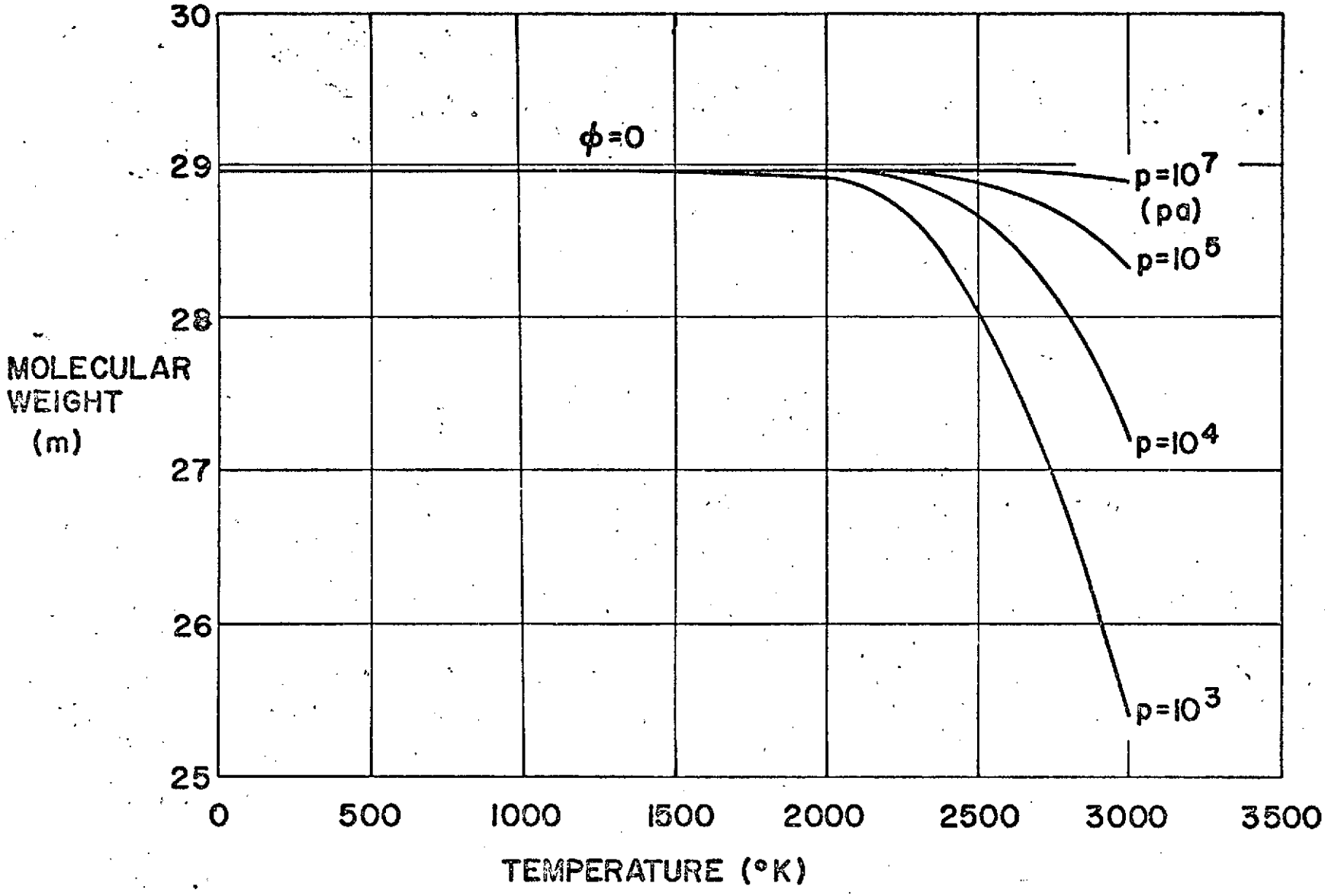

FIGURE A6. MOLECULAR WEIGHT AS A FUNCTION OF TEMPERATURE AND PRESSURE.

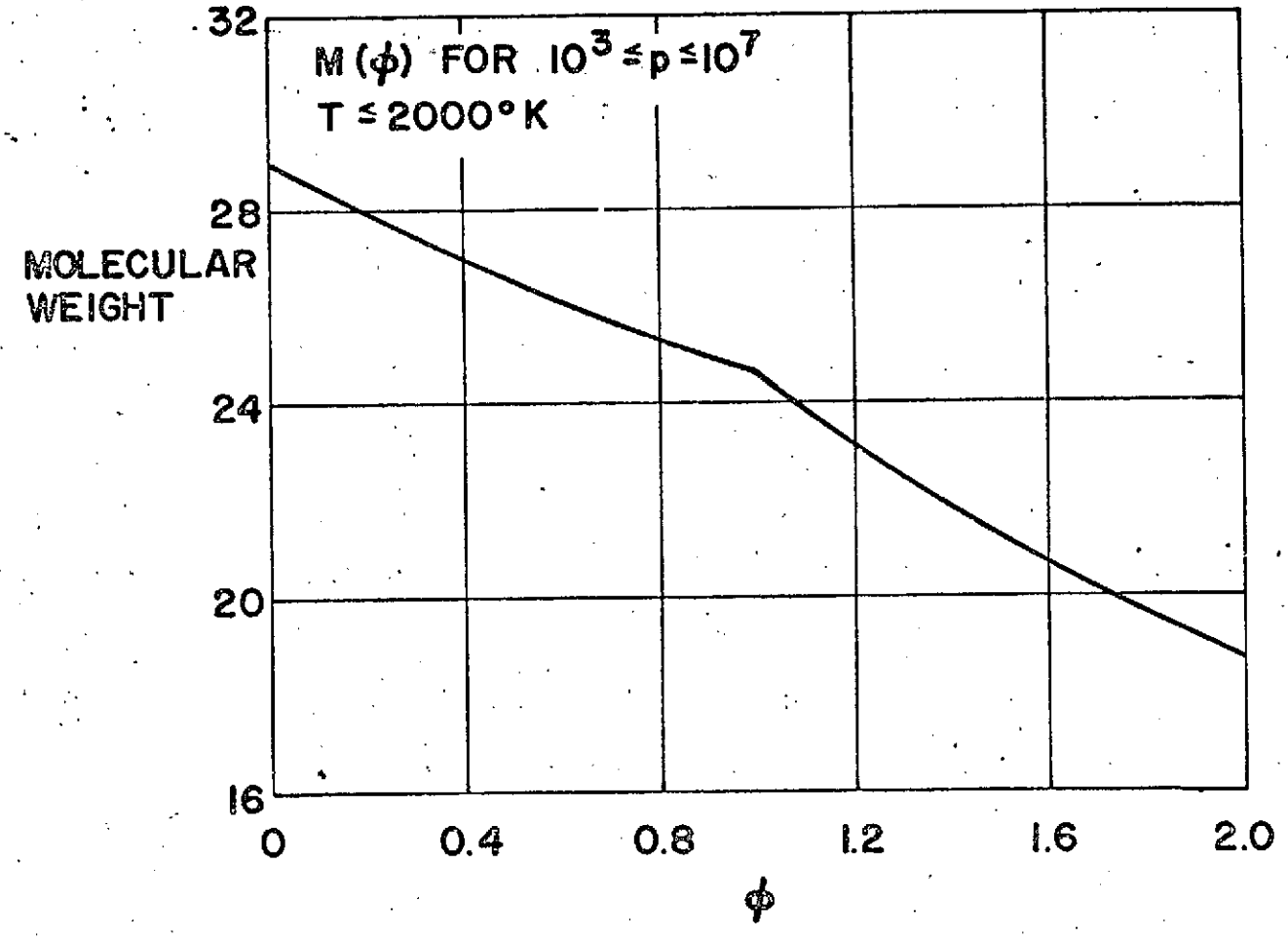

FIGURE A7. MOLECULAR WEIGHT AS A FUNCTION OF EQUIVALENCE RATIO FOR T≤2000°K.

and

$$d_2 = a_2 \left(\frac{\ln p}{2.3}\right)^{1.5} + b_2 \left(\frac{\ln p}{2.3}\right) + c_2 \qquad \text{(IIb.23)}$$

For $0 \le \phi \le 1$ (IIb.24)

$$a_2 = -2.3\phi^2 + 4.01\phi + 1.736$$
$$b_2 = 8.61\phi^2 - 15.42\phi - 6.66$$
$$c_2 = -16.88\phi^2 + 33.21\phi + 14.58$$
$$n_2 = .4375\phi^2 + .0625\phi + 2.08$$

and for $1 \le \phi < 2$ (IIb.25)

$$a_2 = -.822\phi^2 + 2.363\phi + 1.905$$
$$b_2 = 2.76\phi^2 - 7.56\phi - 8.68$$
$$c_2 = 3.6\phi^2 + 7.36\phi + 27.15$$
$$n_2 = .47\phi^2 + 1.825\phi + .350$$

APPENDIX III

THRUST, LIFT AND PITCHING MOMENT

In general, the thrust, lift and pitching moment can be defined from the following pressure integral taken over all the nozzle surfaces up to the final X station (XFINAL), i.e.:

$$T_x = \int_A (p-p_\infty)\ \hat{i}_x \cdot d\vec{A}_n \qquad \text{(III.1a)}$$

$$L_y = \int_A (p-p_\infty)\ \hat{i}_y \cdot d\vec{A}_n \qquad \text{(III.1b)}$$

$$M_y = -\int_A (p-p_\infty)\ \hat{i}_y \cdot x d\vec{A}_n + \int_A (p-p_\infty)\ \hat{i}_x \cdot y d\vec{A}_n \qquad \text{(III.1c)}$$

where the coordinate system and vehicle configuration are depicted in Figure (III-1).

However, since the lateral geometry of the nozzle is treated approximately, it is not possible to determine the lateral contributions to the above integrals by direct pressure integration. The use of the integral conservation theorems provides, however, an alternate means of defining the thrust, lift and pitching moment.

For a fixed control volume

$$\Sigma \vec{F} = \int_A \vec{q}\ (\rho \vec{q}) \cdot \hat{n} dA \qquad \text{(III.2a)}$$

$$\Sigma \vec{F} \times \vec{r} = \int_A (\vec{q} \times \vec{r})\ (\rho \vec{q}) \cdot \hat{n} dA \qquad \text{(III.2b)}$$

where the integrals extend over the throat area and a suitably defined nozzle exit area. Care must be exercised in using Equations (III.2) since small errors in mass flow can produce large errors in net thrust, lift and pitching moment.

By straightforward algebraic manipulation and use of the Equation of State and the definition of the local sound speed Equations (III.2) may be reduced to the following:

$$T_x = \int_{A_{exit}} \frac{(\gamma p M^2 \sin(\theta_s-\theta)\cos\theta + (p-p_\infty)\sin\theta_s)}{\sin\theta_s}\, dydz$$

$$- \int_{A_{throat}} \frac{(\gamma p M^2 \sin(\theta_s-\theta)\cos\theta + (p-p_\infty)\sin\theta_s)}{\sin\theta_s}\, dydz \qquad \text{(III.3a)}$$

$$L_y = \int_{A_{exit}} \frac{(\gamma p M^2 \sin(\theta_s-\theta)\sin\theta + (p-p_\infty)\cos\theta_s)}{\sin\theta_s}\, dydz$$

$$- \int_{A_{throat}} \frac{(\gamma p M^2 \sin(\theta_s-\theta)\sin\theta + (p-p_\infty)\cos\theta_s)}{\sin\theta_s}\, dydz \qquad \text{(III.3b)}$$

$$M_y = \left[\int_{A_{exit}} \frac{(\gamma p M^2 \sin(\theta_s-\theta)\cos\theta + (p-p_\infty)\sin\theta_s)}{\sin\theta_s} \, y\,dy\,dz \right.$$

$$\left. - \int_{A_{throat}} \frac{(\gamma p M^2 \sin(\theta_s-\theta)\cos\theta + (p-p_\infty)\sin\theta_s)}{\sin\theta_s} \, y\,dy\,dz \right] \qquad \text{(III.3c)}$$

$$- \left[\int_{A_{exit}} \frac{(\gamma p M^2 \sin(\theta_s-\theta)\sin\theta + (p-p_\infty)\cos\theta_s)}{\sin\theta_s} \, x\,dy\,dz \right.$$

$$\left. - \int_{A_{throat}} \frac{(\gamma p M^2 \sin(\theta_s-\theta)\sin\theta + (p-p_\infty)\cos\theta_s)}{\sin\theta_s} \, x\,dy\,dz \right]$$

where θ_s is the local inclination of the throat or exit area and z is the lateral extent of the nozzle. The algebraic differences between Equations (III.2) and (III.3) represent the integrated force and moment contributions of the sidewalls/and or fences. If no fences are present the momentum balance is carried out at the cowl exit station but the pressure integrations are still computed over the full vehicle and cowl surfaces.

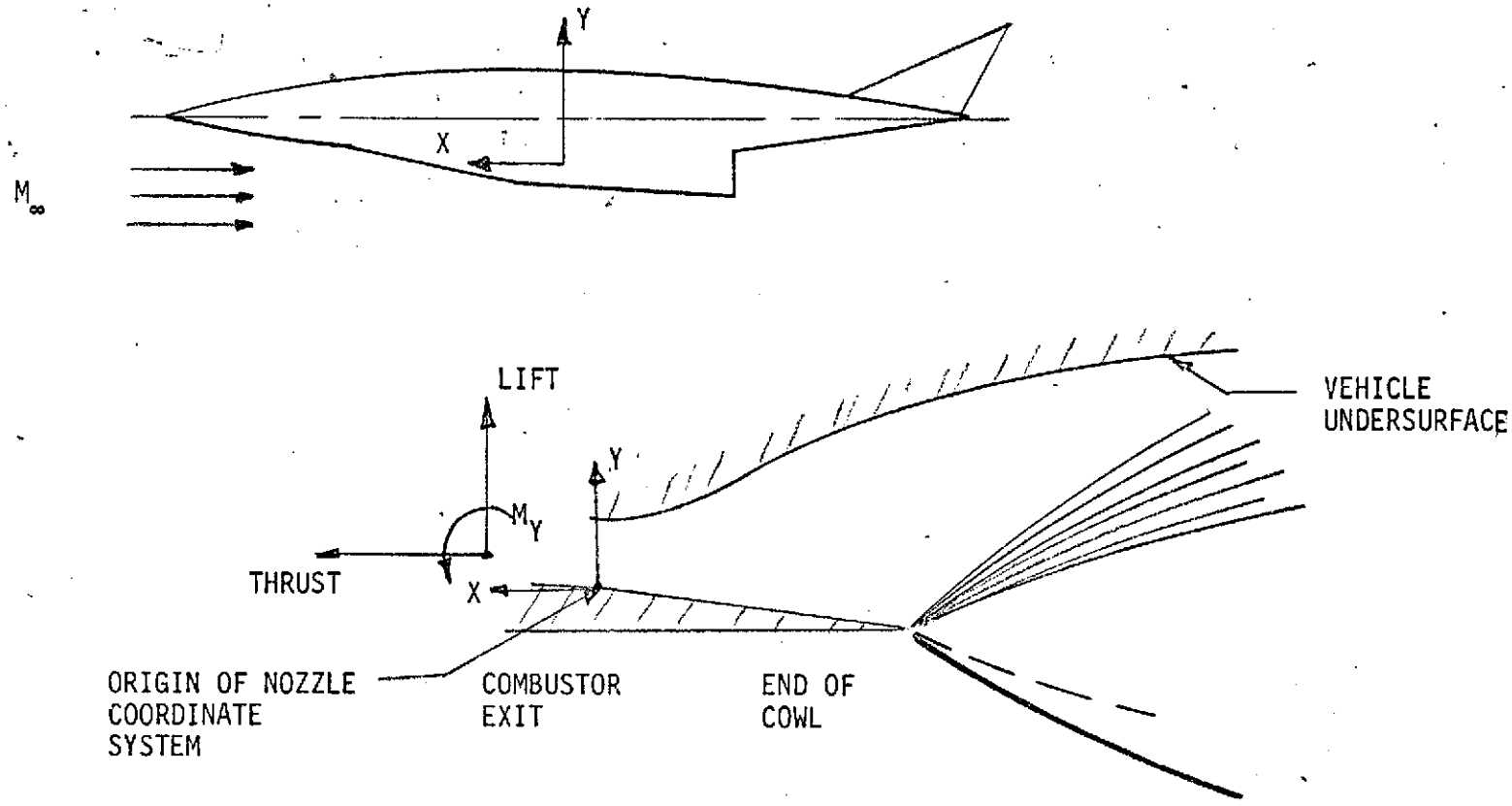

FIGURE III-1. THRUST, LIFT, MOMENT